Inorg. Chem. **2009**, *48*, 1132−1147

Complexation of Trivalent Lanthanides with Planar Tridentate Aromatic Ligands Tuned by Counteranions and Steric Constraints

Aude Escande, Laure Guénée,* Kerry-Lee Buchwalder, and Claude Piguet*

Department of Inorganic, Analytical and Applied Chemistry, University of Geneva, 30 quai E. Ansermet, CH-1211 Geneva 4, Switzerland

Received October 7, 2008

Among the plethora of parameters controlling the stability and structures of lanthanide coordination complexes, it is often difficult to decipher their relative importance in the global complexation processes. The combination of the *bond valence* method (for analyzing solid state structures) with the thermodynamic *site binding* model (for unravelling complexation reactions occurring in solution) appears to be an efficient tool for specifically addressing interligand effects, which affect the output of the coordination process. When applied to the reaction of the tridentate aromatic scaffolds 2,2′:6′,2″-terpyridine (**L1**) and 2,6-bis(benzimidazol-2-yl)pyridine (**L2**) with trivalent lanthanides, Ln(III), we demonstrate that the successive fixation of ligands, eventually leading to the triple-helical complexes $[Ln(\mathbf{L}\boldsymbol{k})_3]^{3+}$, is anticooperative both in the solid state and in solution, with a special sensitivity to the nature of the counteranion and to the peripheral substitution for **L2**. Consequently, in addition to the classical entropic driving forces resulting from the use of specific metal/ligand ratio, the stoichiometry of the final complex can be tuned by a judicious choice of interligand interactions, as exemplified by the unusual isolation of stable complexes with Ln/**L** = 2:3 ratios.

Introduction

In polar organic solvents, planar tridentate aromatic ligands possessing three heterocyclic nitrogen donor atoms such as 2,2′:6′,2″-terpyridine (**L1**),[1−9] 2,6-bis(1-methylbenzimidazol-2-yl)pyridine (**L2**),[10,11] or 2,6-bis([1,2,4]-triazine-3-yl)pyridine (**L3**)[12−14] can displace solvent molecules and/or anions from the first coordination sphere of trivalent lanthanide salts, LnX_3, to give a plethora of $[Ln(\mathbf{L}\boldsymbol{k})_nX_3]$ complexes (n = 1−3), whose compositions depend on the metal−ligand stoichiometric ratios and on the nature of the counteranions (Chart 1).

With coordinating nitrate anions ($X = NO_3^-$), the complexation process is dominated by the formation of 1:1 complexes $[Ln(\mathbf{L}\boldsymbol{k})(NO_3)_3]$ in solution because the bidentate nitrates are thought to tightly interact with the metal, thus preventing the complexation of additional tridentate ligands.[3,4,6,8−10,12−14] However, some anion transfers have been described leading to intricate mixtures of solvated species with 1:1 ($[Ln(\mathbf{L}\boldsymbol{k})(NO_3)_2]^+$, $[Ln(\mathbf{L}\boldsymbol{k})(NO_3)_4]^-$) and 1:2 stoichiometries ($[Ln(\mathbf{L}\boldsymbol{k})_2(NO_3)_2]^+$).[3] A similar behavior is observed with carboxylate anions ($X = RCO_2^-$), except for the tendency of these counteranions to act as bridging

* To whom correspondence should be addressed. E-mail: Laure.Guenee@unige.ch (L.G.); Claude.Piguet@unige.ch (C.P.).

(1) Durham, D. A.; Frost, G. H.; Hart, F. A. *J. Inorg. Nucl. Chem.* **1969**, *31*, 833–838.
(2) Chapman, R. D.; Loda, R. T.; Riehl, J. P.; Schwartz, R. W. *Inorg. Chem.* **1984**, *23*, 1652–1657.
(3) Fréchette, M.; Bensimon, C. *Inorg. Chem.* **1995**, *34*, 3520–3527.
(4) Semenova, L. I.; White, A. H. *Aust. J. Chem.* **1999**, *52*, 507–517.
(5) Semenova, L. I.; Sobolev, A. N.; Skelton, B. W.; White, A. H. *Aust. J. Chem.* **1999**, *52*, 519–529.
(6) Drew, M. G. B.; Iveson, P. B.; Hudson, M. J.; Liljenzin, J. O.; Spjuth, L.; Cordier, P.-Y.; Enarsson, A.; Hill, C.; Madic, C. *J. Chem. Soc., Dalton Trans.* **2000**, 821–830.
(7) Mürner, H.-R.; Chassat, E.; Thummel, R. P.; Bünzli, J.-C. G. *J. Chem. Soc., Dalton Trans.* **2000**, 2809–2816.
(8) Ionova, G.; Rabbe, C.; Guillaumont, R.; Ionov, S.; Madic, C.; Krupa, J.-C.; Guillaneux, D. *New J. Chem.* **2002**, *26*, 234–242.
(9) Ahrens, B.; Cotton, S., A.; Feeder, N.; Noy, O. E.; Raithby, P. R.; Teat, S. J *J. Chem. Soc., Dalton Trans.* **2002**, 2027–2030.
(10) Piguet, C.; Williams, A. F.; Bernardinelli, G.; Moret, E.; Bünzli, J.-C. G. *Helv. Chim. Acta* **1992**, *75*, 1697–1717.
(11) Piguet, C.; Bünzli, J.-C. G.; Bernardinelli, G.; Williams, A. F. *Inorg. Chem.* **1993**, *32*, 4139–4149.
(12) Drew, M. G. B.; Hill, C.; Hudson, M. J.; Iveson, P. B.; Madic, C.; Youngs, T. G. A. *Dalton Trans.* **2004**, 244–251.
(13) Foreman, M. R. S.; Hudson, M. J.; Drew, M. G. B.; Hill, C.; Madic, C. *Dalton Trans.* **2006**, 1645–1653.
(14) Hudson, M. J.; Boucher, C. E.; Braekers, D.; Desreux, J. F.; Drew, M. G. B.; Foreman, M. R. S. J.; Harwood, L. M.; Hill, C.; Madic, C.; Marken, F.; Youngs, T. G. A. *New J. Chem.* **2006**, *30*, 1171–1183.

10.1021/ic801908c CCC: $40.75
Published on Web 01/09/2009

Chart 1

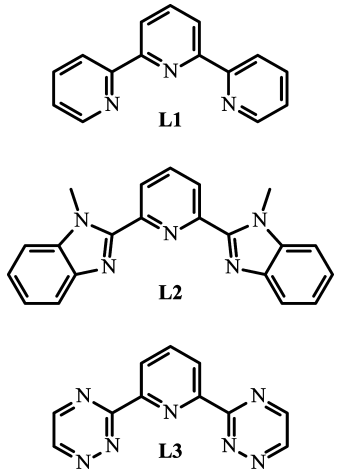

bidentate ligands.[15−18] The hydrated halides $LnX_3 \cdot 6H_2O$ (X = Cl, Br) have also been reacted with **L1** along the complete lanthanide series, but the use of water as a cosolvent for imperious solubility reasons, limits complexation to 1:1 adducts of formulas $[Ln(\mathbf{L1})Cl(H_2O)_5]Cl_2$[19] and $[Ln(\mathbf{L1})(H_2O)_n]Br_3$ (n = 5, 6).[20] It is only with noncoordinating perchlorates in poorly competiting acetonitrile that 1:2 $[Ln(\mathbf{Lk})_2(CH_3CN)_n]^{3+}$ and triple-helical 1:3 $[Ln(\mathbf{Lk})_3]^{3+}$ complexes can be easily prepared in solution and in the solid state.[1,2,5,7,11] The crystal structures of $[Eu(\mathbf{L1})_3](ClO_4)_3$[1] and $[Eu(\mathbf{L2})_3](ClO_4)_3$[11] unambigously show the replacement of all solvent molecules and counteranions with the nine heterocyclic nitrogen atoms of the three tridentate ligands. However, the solution structure of $[Ln(\mathbf{L1})_3]^{3+}$ evidences partial and dynamic on−off decomplexation of the distal pyridine rings of the ligand,[2] while paramagnetic NMR data collected for $[Ln(\mathbf{L2})_3]^{3+}$ (Ln = Ce−Yb) indicate that the triple-helical structure is maintained in acetonitrile only for the larger lanthanides (Ln = La−Dy).[21] The improved stability and kinetic inertness of $[Ln(\mathbf{L2})_3]^{3+}$ have been tentatively assigned to the replacement of the two distal six-membered pyridine rings in **L1** with five-membered imidazole rings in **L2**, which produces a larger coordination cavity, better suited for trivalent lanthanides.[10,11,21,22] Moreover, the 2,6-bis(benzimidazol-2-yl)pyridine backbone in **L2** is easier to derivatize[23] than terpyridine,[24] which allows its facile incorporation into extended segmental ligands for the design of polynuclear luminescent helicates[25] and lipophilic liquid crystal scaffolds.[26,27] Subtle stereoelectronic effects can be then induced by a judicious substitution of the aromatic backbone ($\mathbf{L2^{a-n}}$, Chart 2). A stepwise increase of the steric bulk at the R^2 position along the $\mathbf{L2^{a-b-c-d-e}}$ series increasingly affects the coplanarity of the three aromatic rings in the final complexes, which severely limits their stabilities in solution.[11,21,28,29] An even more dramatic effect is obtained when alkyl groups are connected close to the coordination cavity at the R^5 positions, and $\mathbf{L2^g}$ shows no detectable affinity for Ln(III).[22] Substitution at the remote R^3 and R^4 positions in $\mathbf{L2^{k-n}}$ restores a standard coordination behavior toward Ln(III).[22,30−32] We however notice that the thermodynamic formation constants of the lipophilic 1:1 complexes $[Ln(\mathbf{L2^{k-n}})X_3]$ may vary by 1−2 orders of magnitude depending on the counteranions (X = NO_3^- or X = $CF_3CO_2^-$) or on the solvents (CH_2Cl_2 or CH_2Cl_2/CH_3CN).[33] Although less striking, the substitution of the central pyridine ring in $\mathbf{L2^i}$[34] and $\mathbf{L2^j}$[35] may further contribute to some fine-tuning of the affinity of the tridentate binding unit for Ln(III).

This set of empirical observations suggests that the stoichiometries, stabilities, and structures of the final lanthanide complexes with **L2**-type tridentate ligands could be rationally controlled and predicted according that some reliable molecular structural and energetic descriptors are at hand. As a first step toward this goal, we propose in this contribution (i) to exploit the bond valence method for quantifying metal−ligand affinities and ligand distortions in the solid state,[36−40] and (ii) to concomitantly use the thermodynamic site binding model for addressing these

(15) Kepert, C. J.; Lu, W.-M.; Semenova, L. I.; Skelton, B. W.; White, A. H. *Aust. J. Chem.* **1999**, *52*, 481–496.
(16) Nozary, H.; Piguet, C.; Rivera, J.-P.; Tissot, P.; Bernardinelli, G.; Vulliermet, N.; Weber, J.; Bünzli, J.-C. G. *Inorg. Chem.* **2000**, *39*, 5286–5298.
(17) Nozary, H.; Piguet, C.; Rivera, J.-P.; Tissot, P.; Morgantini, P.-Y.; Weber, J.; Bernardinelli, G.; Bünzli, J.-C. G.; Deschenaux, R.; Donnio, B.; Guillon, D. *Chem. Mater.* **2002**, *14*, 1075–1090.
(18) Nozary, H.; Torelli, S.; Guénée, L.; Terazzi, E.; Bernardinelli, G.; Donnio, B.; Guillon, D.; Piguet, C. *Inorg. Chem.* **2006**, *45*, 2989–3003.
(19) Kepert, C. J.; Weimin, L.; Skelton, B. W.; White, A. H. *Aust. J. Chem.* **1994**, *47*, 365–384.
(20) Semenova, L. I.; White, A. J. *Aust. J. Chem.* **1999**, *52*, 539–550.
(21) Petoud, S.; Bünzli, J.-C. G.; Renaud, F.; Piguet, C.; Schenk, K. J.; Hopfgartner, G. *Inorg. Chem.* **1997**, *36*, 5750–5760.
(22) Piguet, C.; Bünzli, J.-C. G.; Bernardinelli, G.; Bochet, C. G.; Froidevaux, P. *J. Chem. Soc., Dalton Trans.* **1995**, 83–97.
(23) Piguet, C.; Bocquet, B.; Hopfgartner, G. *Helv. Chim. Acta* **1994**, *77*, 931–942.
(24) Cargill Thompson, A. M. W. *Coord. Chem. Rev.* **1997**, *160*, 1–52.
(25) Dalla Favera, N.; Hamacek, J.; Borkovec, M.; Jeannerat, D.; Gumy, F.; Bünzli, J.-C. G.; Ercolani, G.; Piguet, C. *Chem.—Eur. J.* **2008**, *14*, 2994–3005, and references therein.
(26) Piguet, C.; Bünzli, J.-C. G.; Donnio, B.; Guillon, D. *Chem. Commun.* **2006**, 3755–3768.
(27) McKenzie, B. M.; Miller, A. K.; Wojtecki, R. J.; Johnson, J. C.; Burke, K. A.; Tzeng, K. A.; Mather, P. T.; Rowan, S. J. *Tetrahedron* **2008**, *64*, 8488–8495.
(28) Muller, G.; Bünzli, J.-C. G.; Schenk, K. J.; Piguet, C.; Hopfgartner, G. *Inorg. Chem.* **2001**, *40*, 2642–2651.
(29) Muller, G.; Maupin, C. L.; Riehl, J. P.; Birkedal, H.; Piguet, C.; Bünzli, J.-C. G. *Eur. J. Inorg. Chem.* **2003**, *406*, 5–4072.
(30) Terazzi, E.; Torelli, S.; Bernardinelli, G.; Rivera, J.-P.; Bénech, J.-M.; Bourgogne, C.; Donnio, B.; Guillon, D.; Imbert, D.; Bünzli, J.-C. G.; Pinto, A.; Jeannerat, D.; Piguet, C. *J. Am. Chem. Soc.* **2005**, *127*, 888–903.
(31) Escande, A.; Guénée, L.; Nozary, H.; Bernardinelli, G.; Gumy, F.; Aebischer, A.; Bünzli, J.-C. G.; Donnio, B.; Guillon, D.; Piguet, C. *Chem.—Eur. J.* **2007**, *13*, 8696–8713.
(32) Terazzi, E.; Guénée, L.; Morgantini, P.-Y.; Bernardinelli, G.; Donnio, B.; Guillon, D.; Piguet, C. *Chem.—Eur. J.* **2007**, *13*, 1674–1691.
(33) Nozary, H.; Torelli, S.; Guénée, L.; Terazzi, E.; Bernardinelli, G.; Donnio, B.; Guillon, D.; Piguet, C. *Inorg. Chem.* **2006**, *45*, 2989–3003.
(34) Petoud, S.; Bünzli, J.-C. G.; Schenk, K. J.; Piguet, C. *Inorg. Chem.* **1997**, *36*, 1345–1353.
(35) Muller, G.; Riehl, J. P.; Schenk, K. J.; Hopfgartner, G.; Piguet, C.; Bünzli, J.-C. G. *Eur. J. Inorg. Chem.* **2002**, *310*, 1–3110.
(36) Pauling, L. *J. Am. Chem. Soc.* **1929**, *51*, 1010–1026.
(37) Brown, I. D.; Altermatt, D. *Acta Crystallogr. B* **1985**, *B41*, 244–247.
(38) Breese, N. E.; O'Keeffe, M. *Acta Crystallogr. B* **1991**, *B47*, 192–197.
(39) Brown, I. D. *Acta Crystallogr. B* **1992**, *B48*, 553–572.
(40) Brown, I. D. *The Chemical Bond in Inorganic Chemistry*; Oxford University Press: Oxford, U.K., 2002.

Chart 2

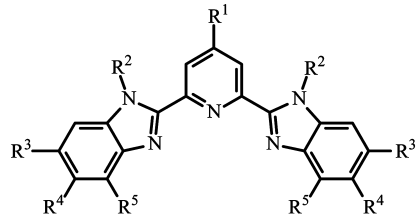

Ligand	R^1	R^2	R^3	R^4	R^5	Ref
L2	H	CH_3	H	H	H	10
L2[a]	H	C_2H_5	H	H	H	11
L2[b]	H	C_3H_7	H	H	H	11
L2[c]	H	C_8H_{17}	H	H	H	10
L2[d]	H	$(CH_3O)_2C_6H_5$	H	H	H	11
L2[e]	H		H	H	H	28
L2[f]	H	C_2H_5	H	CH_3	H	22
L2[g]	H	C_2H_5	H	H	CH_3	22
L2[h]	H	C_2H_5	H	OCH_3	H	30
L2[i]	$PhNEt_2$	CH_3	H	H	H	34
L2[j]	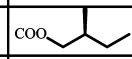	CH_3	H	H	H	35
L2[k]	H	C_2H_5	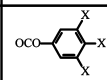	H	H	30
L2[l]	H	C_2H_5	H	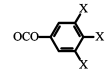	H	30
L2[m]	H	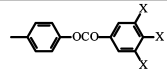	H	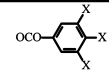	H	31
L2[n]	H	C_2H_5	H	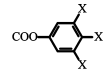	H	32

characteristics in solution.[41,42] The combination of both approaches provides a new tool for analyzing and designing lanthanide coordination complexes with preorganized ligands.

Results and Discussion

Solid-State Structures and Bond Valence Sum Analysis. The bond valence method refers to the original concept of electrostatic valence developped by Pauling,[36] which applies to inorganic salts made up of packed cations and anions. According to this theory, each cation i is surrounded by n_i anions held at a fixed distance. Its positive charge z_i (in electrostatic units) is equally distributed onto each anion according to $v_i = z_i/n_i$. Since each anion shares the vertices of several coordination polyhedra, the total electrostatic valence per anion is given by $\xi = \sum_i z_i/n_i$, which indeed corresponds to the absolute total charge of the anion. Following and extending this strategy, the bond valence method assigns a bond valence (v_{ij}) to each interacting pair formed by a donor j and a central atom i; v_{ij} is related to the bond length of the interacting pair (d_{ij}) according to eq 1,[37−40] whereby R_{ij} is known as the bond valence parameter, which only depends on the pair of interacting atoms, and b = 0.37 Å is a universal scaling constant.[37]

$$v_{ij} = e^{[(R_{ij}-d_{ij})/b]} \quad (1)$$

In a manner similar to that of the formal charge borne by the anion in Pauling's model is given by the sum of the delocalized charge of the central atom, the bond valence sum (V_i, eq 2) in the bond valence method, corresponds to the formal oxidation state of the central atom i.[38,39]

$$V_i = \sum_j v_{ij} \quad (2)$$

Since a reliable set of R_{ij} parameters for Ln−O[43] and Ln−N[44] bonds involved in metal−organic complexes has been recently computed, along the complete lanthanide series, the

(41) Piguet, C.; Borkovec, M.; Hamacek, J.; Zeckert, K. *Coord. Chem. Rev.* **2005**, *249*, 705–726.
(42) Hamacek, J.; Borkovec, M.; Piguet, C. *Dalton Trans.* **2006**, 1473–1490.

bond valence method can be applied in lanthanide complexes for unravelling geometrical strains in solid-state structures, which are responsible for deviations from the bond valence sum $V_i = 3$ expected for Ln(III).[45−47] We thus first focus on the series [Eu(**L2**)$(NO_3)_3$(MeOH)],[10] [Lu(**L2**)$_2(OH_2)$-(MeOH)]$^{3+}$,[11] and [Eu(**L2**)$_3$]$^{3+}$[11] complexes (Table S1−S3, Supporting Information), in which **L2** is a nonconstrained tridentate ligand bearing methyl groups bound to the noncoordinating nitrogen atoms of the distal benzimidazole rings (entries 1, 6, and 10 in Table 1).

The bond valence sum gradually decreases from $V_{Eu} = 3.04$ (Ln/**L2** = 1:1) to $V_{Lu} = 2.93$ (Ln/**L2** = 1:2) and $V_{Eu} = 2.80$ (Ln/**L2** = 1:3), a variation beyond the maximum tolerance established by a comprehensive analysis of the lanthanide structures contained in the Cambridge Data Base ($V_{Ln} = 3.0 \pm 0.1$),[43,44] but within the range of the maximum deviation accepted for a correct structure ($V_{Ln} = 3.0 \pm 0.3$).[45] This variation results from (i) a global increase of the Ln−N bond length on going from 1:1 to 1:3 complexes, together with (ii) a smaller dispersion of the bond valence $\nu_{N\text{-ligand}}$arising from the nitrogen atoms of the benzimidazole rings and of the pyridine rings (the inequality $\nu_{N\text{-pyridine}} < \nu_{N\text{-benzimidazole}}$ is maximum for the 1:1 stoichiometry). This behavior is confirmed in the second homologous series [Eu(**L2**^{e})-$(NO_3)_3(CH_3CN)$],[29] [La(**L2**^{e})$_2(OH_2)(ClO_4)_2]^+$,[28] and [Eu(**L2**^{e})$_3$]$^{3+}$[28] with the sterically hindered ligand **L2**^{e} (entries 2, 7, and 11 in Table 1 and Tables S4−S6, Supporting Information), for which the noncoordinating nitrogen atoms of the benzimidazole rings are grafted with neopentyl residues (Chart 2). To further substantiate these observations, we have explored the complexation reactions of **L2**^{a}, a ligand possessing intermediate steric constraints between **L2** and **L2**^{e}, with Lu$(Otf)_3\cdot 3H_2O$ (Otf$^-$ = $CF_3SO_3^-$), Lu$(SCN)_3\cdot 3H_2O\cdot C_2H_5OH$, and $LuCl_3\cdot 6H_2O$ in polar organic solvents. The reaction of **L2**^{a} with lanthanide chloride salts gives 1:1 complexes, even in excess of ligand (see next section for stabilities in solution). X-ray quality crystals of [Lu(**L2**^{h})$(H_2O)_5]Cl_3\cdot CH_3NO_2$ (**1**) can be obtained upon slow diffusion of diisopropylether into a concentrated nitromethane solution containing the analogous but more soluble ligand **L2**^{h} with $LuCl_3\cdot 6H_2O$ in a 1:1 stoichiometric ratio. The crystal structure of **1** is composed of eight-coordinate [Lu(**L2**^{h})$(H_2O)_5]^{3+}$ cations, ionic chloride anions (whose location within the unit cell provides a noncentrosymmetric structure, Flack parameter $x = 0.0067(6)$), and noncoordinated disordered nitromethane molecules (see Experimental Section). Except for their participation in a three-dimensional network of hydrogen bonds with the coordinated water molecules (Figure S1 and Table S21, Supporting Information), the chloride anions show no other feature of interest, but we

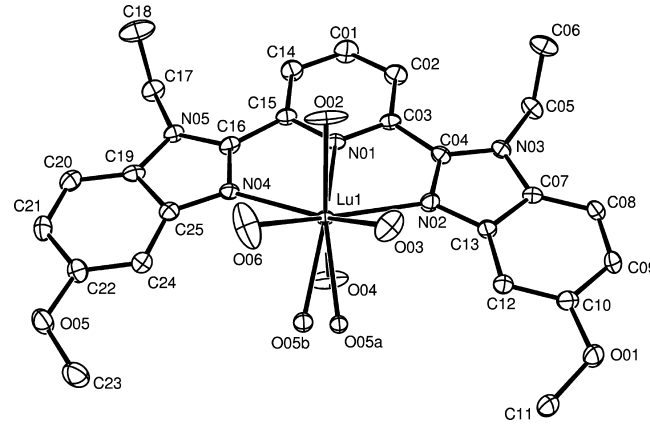

Figure 1. Perspective view of [Lu(**L2**^{h})$(H_2O)_5]^{3+}$ in the crystal structure of **1** with numbering scheme. Ellipsoids are represented at the 40% probability level.

notice that water molecules efficiently compete with chloride anions for coordination to Lu(III). The molecular structure of the cation shows the expected meridional tricoordination of the aromatic ligand **L2**^{h} to Lu(III), with a central Lu−N(pyridine) bond length significantly longer (0.071(3) Å) than the distal Lu−N(benzim) bond lengths (Figure 1 and Table 2).

This translates into bond valences of $\nu_{N\text{-py}} = 0.31$ and $\nu_{N\text{-bzim}} = 0.37-0.39$ (py = pyridine, bzim = benzimidazole; Table S7, Supporting Information), a trend in line with that observed in the parent complexes [Eu(**L2**)$(NO_3)_3$(MeOH)] ($\nu_{N\text{-py}} = 0.30$ and $\nu_{N\text{-bzim}} = 0.36-0.43$, Table S1, Supporting Information)[10] and [Eu(**L2**^{e})$(NO_3)_3(CH_3CN)$] ($\nu_{N\text{-py}} = 0.29$ and $\nu_{N\text{-bzim}} = 0.43$, Table S4, Supporting Information),[29] which is characteristic of an almost coplanar arrangement of the three aromatic rings (py-bzim interplane angles = 3.57(9)° and 5.7(1)° in [Lu(**L2**^{h})$(H_2O)_5]^{3+}$, Table S22, Supporting Information). The Ln−O bond lengths in [Lu(**L2**^{h})$(H_2O)_5]^{3+}$ do not significantly deviate from the average value 2.31(2) Å, and the five O-donor atoms complete a distorted dodecahedral Lu(III) coordination sphere (Figure 1). The ionic radius of Lu(III) calculated according to Shannon's definition with r(N) = 1.46 Å and r(O−water) = 1.35 Å amounts to $R^{Lu}_{CN=8} = 0.967$ Å, in fair agreement with 0.977 Å expected for eight-coordinated Lu(III).[48]

When chloride counteranions are replaced with triflates in Lu$(Otf)_3\cdot 3H_2O$, reaction with **L2**^{a} in acetonitrile gives 1:1, 1:2, and 1:3 complexes (see next section for stabilities in solution). Upon a strict control of the stoichiometry, X-ray quality prisms of [Lu(**L2**^{a})$(Otf)_3(CH_3CN)(H_2O)$] (**2**) and [Lu(**L2**^{a})$_2$(Otf)(H_2O)](Otf)$_2$ (**3**) can be obtained from concentrated acetonitrile/diisopropylether solutions. In **2**, the Lu(III) atom is eight-coordinated by one tridentate ligand **L2**^{a}, three monodentate triflate anions, one water, and one acetonitrile molecule (Figure 2). Interestingly, the py-bzim interplane angles in the coordinated ligand (12.4(1)° and 20.8(1)°, Table S23, Supporting Information) are large enough to produce a roof-shaped arrangement of the three aromatic rings, but bond lengths (Table 3), and consequently, the bond valences (Table S8, Supporting Information) are

(43) Trzesowska, A.; Kruszynski, R.; Bartczak, T. J. *Acta Crystallogr. B* **2004**, *B60*, 174–178.
(44) Trzesowska, A.; Kruszynski, R.; Bartczak, T. J. *Acta Crystallogr B* **2005**, *B61*, 429–434.
(45) Palenik, G. J. *Inorg. Chem.* **2003**, *42*, 2725–2728.
(46) Brown, I, D. *Acta Crystallogr. B* **1977**, *B33*, 1305–1310.
(47) Jensen, W. P.; Palenik, G. J.; Tiekink, E. R. T. *Polyhedron* **2001**, *20*, 2137–2143.
(48) Shannon, R. D. *Acta Crystallogr.* **1976**, *A32*, 751–767.

Table 1. Average Bond Valences (ν_{ij}, eq 1) and Bond Valence Sums (V_i, eq 2) in the Crystal Structures of 1:1, 1:2, and 1:3 Complexes of **L2**, **L2**^{a}, **L2**^{e}, **L2**^{f}, and **L2**^{h} with Trivalent Lanthanides (Otf = triflate, O-Solv = H_2O or CH_3OH, N-solv = CH_3CN)

complexes	Ln/**L**	$\nu_{N\text{-ligand}}$	$\nu_{N\text{-NCS}}$	$\nu_{N\text{-Solv}}$	$\nu_{O\text{-NO3}}$	$\nu_{O\text{-Otf}}$	$\nu_{O\text{-ClO4}}$	$\nu_{O\text{-Solv}}$	V_i	ref
[Eu(**L2**)$(NO_3)_3(CH_3OH)$]	1:1	0.36(6)			0.28(5)			0.29	3.04	10
[Eu(**L2**^{e})$(NO_3)_3(CH_3CN)$]	1:1	0.38(9)		0.21	0.27(3)				2.99	29
[Lu(**L2**^{a})$(Otf)_3(CH_3CN)(H_2O)$]	1:1	0.35(4)		0.37		0.36(4)			2.90	this work
[Lu(**L2**^{h})$(H_2O)_5]^{3+}$	1:1	0.35(4)						0.37(2)	2.92	this work
[Lu(**L2**^{a})$(SCN)_4]^{-}$	1:1	0.35(4)	0.51(2)						3.07	this work
[Lu(**L2**$)_2(H_2O)(CH_3OH)]^{3+}$	1:2	0.37(4)						0.37(4)	2.93	11
[La(**L2**^{e}$)_2(ClO_4)_2(H_2O)]^{+}$	1:2	0.33(4)					0.25(2)	0.28	3.00	28
[Lu(**L2**^{a}$)_2(Otf)(H_2O)]^{2+}$	1:2	0.34(3)				0.36		0.40	2.83	this work
[Lu(**L2**^{a}$)_2(SCN)_2]^{+}$	1:2	0.31(4)	0.47(2)						2.81	this work
[Eu(**L2**$)_3]^{3+}$	1:3	0.31(2)							2.80	11
[Eu(**L2**^{e}$)_3]^{3+}$	1:3	0.32(2)							2.87	28
[Eu(**L2**^{f}$)_3]^{3+}$	1:3	0.32(3)							2.84	22

Table 2. Selected Bond Distances (Å) and Angles (deg) for [Lu(**L2**^{h}$)(H_2O)_5]Cl_3\cdot CH_3NO_2$ (**1**)

		bond distances			
Lu−N01	2.479(3)	Lu−O02	2.288(3)	Lu−O05a	2.313(5)
Lu−N02	2.397(3)	Lu−O03	2.334(3)	Lu−O05b	2.296(5)
Lu−N04	2.419(3)	Lu−O04	2.302(3)	Lu−O06	2.345(3)
		N−Lu−N bite angles			
N01−Lu−N02	66.3(1)	N01−Lu−N04	66.1(1)	N02−Lu−N04	130.2(1)
		N−Lu−O angles			
N01−Lu−O02	72.8(1)	N01−Lu−O03	127.1(1)	N01−Lu−O04	79.2(1)
N01−Lu−O06	130.2(1)	N01−Lu−O05a	145.5(1)	N01−Lu−O05b	146.9(1)
N02−Lu−O02	89.9(1)	N02−Lu−O03	74.9(1)	N02−Lu−O04	79.0(1)
N02−Lu−O06	150.6(1)	N02−Lu−O05a	95.4(2)	N02−Lu−O05b	113.2(2)
N04−Lu−O02	89.3(1)	N04−Lu−O03	150.0(1)	N04−Lu−O04	78.9(1)
N04−Lu−O06	76.0(1)	N04−Lu−O05a	116.4(2)	N04−Lu−O05b	99.1(1)
		O−Lu−O angles			
O03−Lu−O02	72.7(1)	O03−Lu−O05b	80.9(2)	O03−Lu−O04	127.4(1)
O03−Lu−O05a	69.6(2)	O02−Lu−O05b	138.9(2)	O04−Lu−O02	151.9(1)
O04−Lu−O05b	68.7(2)	O05a−Lu-O02	139.0(1)	O05a−Lu-O05b	18.6(2)
O05a−Lu-O04	68.4(1)	O06−Lu−O02	75.8(1)	O06−Lu−O05b	67.6(2)
O06−Lu−O04	124.5(2)	O06−Lu−O05a	80.1(2)	O06−Lu−O03	76.3(1)

similar to those found for the chloride complex **1** ($\nu_{N\text{-py}}$ = 0.31 and $\nu_{N\text{-bzim}}$ = 0.36−0.38, Table 1). Again, the calculated ionic radius $R^{Lu}_{CN=8}$ = 0.968 Å indicates no special constraint within the metal coordination sphere, and the origin of the distortion of the tridentate ligand in this 1:1 complex remains elusive. We however notice that each water molecule in [Lu(**L2**^{a}$)(Otf)_3(CH_3CN)(H_2O)$] is hydrogen bound to two oxygen atoms of two monodentate triflate anions of a neighboring complex, thus producing chains of packed molecules along *a* direction (Figure S2, Supporting Information).

Closely related distortions of the bound tridentate aromatic

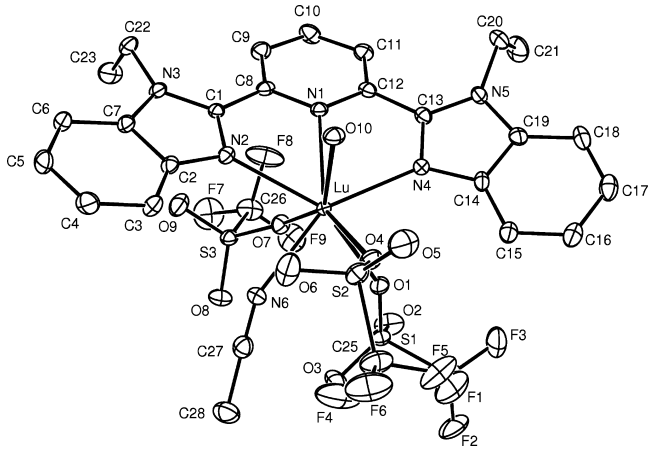

Figure 2. Perspective view of [Lu(**L2**^{a}$)(Otf)_3(CH_3CN)(H_2O)$] in the crystal structure of **2** with numbering scheme. Ellipsoids are represented at the 40% probability level.

L2^{a} ligands are systematically observed in 1:2 and 1:3 complexes, for which interligand constraints are more pronounced. This is illustrated in the crystal structure of the 1:2 complex [Lu(**L2**^{a}$)_2(Otf)(H_2O)](Otf)_2$ (**3**), in which the two tridentate ligands adopt roof-shaped arrangements in the cation [Lu(**L2**^{a}$)_2(Otf)(H_2O)]^{2+}$ (Figure 3, py-bzim interplane angles, 4.7(2)° and 16.7(2)° for ligand a and 23.9(2)° and 24.9(2)° for ligand b, Table S24, Supporting Information). Consequently the Lu−N bond lengths (Table 4) are longer and $\nu_{N\text{-ligand}}$ bond valences are smaller and less dispersed than those obtained when the tridentate ligand adopt a planar arrangement (Table 1 and Table S10, Supporting Information). A monodentate triflate anion and one water molecule complete the eight-coordinate Lu(III) sphere ($R^{Lu}_{CN=8}$ = 0.976 Å), and the total bond valence sum V_i = 2.83 is smaller than in the analogous 1:1 complex (**2**, V_i = 2.90), in agreement with the trend observed with the parent complexes with **L2**. We again notice that the coordinated water molecule is involved in two hydrogen bonds with the oxygen atoms of two triflate anions, whereby one is coordinated to Lu(III) and the second is ionic (Figure S3, Supporting Information).

In the triple-helical 1:3 complexes, the three wrapped tridentate ligands ultimately adopt a significant helical twist induced by successive rotations about the interannular C−C bonds (average pyridine-benzimidazole interplane angle: 25.3(2)° for [Eu(**L2**$)_3]^{3+}$,[11] 26.5(4)° for [Eu(**L2**^{f}$)_3]^{3+}$,[12] and 21(12)° for [Eu(**L2**^{e}$)_3]^{3+}$, Figure 4).[28]

Table 3. Selected Bond Distances (Å) and Angles (deg) for [Lu(**L2**[a])(Otf)$_3$(H$_2$O)(CH$_3$CN)] (**2**)

		bond distances			
Lu−N4	2.400(3)	Lu−N6	2.419(4)	Lu−O10	2.299(3)
Lu−N1	2.482(3)	Lu−O4	2.280(3)	Lu−O1	2.340(3)
Lu−N2	2.424(3)	Lu−O7	2.347(3)		
		N−Lu−N bite angles			
N1−Lu−N2	65.5(1)	N1−Lu−N4	66.3(1)	N2−Lu−N4	128.9(1)
		N−Lu−O angles			
N1−Lu−O4	142.0(1)	N1−Lu−O7	73.3(1)	N1−Lu−O10	76.4(1)
N1−Lu−O1	118.8(1)	N2−Lu−O4	121.8(1)	N2−Lu−O7	77.9(1)
N2−Lu−O10	72.5(1)	N2−Lu−O1	148.6(1)	N4−Lu−O4	87.9(1)
N4−Lu−O7	103.7(1)	N4−Lu−O	1080.7(1)	N4−Lu−O1	72.8(1)
N6−Lu−O4	76.6(1)	N6−Lu−O7	76.6(1)	N6−Lu−O10	116.5(1)
N6−Lu−O1	79.4(1)				
		O−Lu−O angles			
O4−Lu−O10	72.0(1)	O4−Lu−O1	75.6(1)	O4−Lu−O7	142.8(1)
O10−Lu−O1	138.5(1)	O10−Lu−O7	144.2(1)	O1−Lu−O7	74.5(1)

Table 4. Selected Bond Distances (Å) and Angles (deg) for [Lu(**L2**[a])$_2$(Otf)(H$_2$O)](Otf)$_2$ (**3**)

		bond distances			
Lu−N1a	2.474(5)	Lu−N1b	2.504(6)	Lu−O1t	2.325(5)
Lu−N2a	2.436(6)	Lu−N2b	2.412(6)	Lu−O4	2.282(5)
Lu−N4a	2.418(5)	Lu−N4b	2.414(6)		
		N−Lu−N bite angles			
N1a−Lu−N2a	65.2(2)	N1a−Lu−N4a	65.7(2)	N2a−Lu−N4a	126.5(2)
N2b−Lu−N1b	65.7(2)	N1b−Lu−N4b	64.7(2)	N2b−Lu−N4b	128.5(1)
N4b−Lu−N4a	74.3(2)	N4b−Lu−N2a	148.7(2)	N4b−Lu−N1a	115.9(2)
N2b−Lu−N4a	91.5(2)	N2b−Lu−N2a	78.4(2)	N2b−Lu−N1a	101.2(2)
		N−Lu−O angles			
N2b−Lu−O4	94.2(2)	N4b−Lu−O4	83.1(2)	N4a−Lu−O4	154.9(2)
N2a−Lu−O4	78.6(2)	N1a−Lu−O4	136.3(2)	N2b−Lu−O1t	155.9(2)
N4b−Lu−O1t	73.5(2)	N4a−Lu−O1t	105.8(2)	N2a−Lu−O1t	77.8(2)
N1a−Lu−O1t	72.0(2)	N1b−Lu−O4	71.6(2)	N1b−Lu−O1t	129.9(2)
		O−Lu−O angles			
O4−Lu−O1t	77.3(2)				

This considerable distortion of the ligand provides comparable Lu−N bond lengths (Ln−N(py) ≈ Ln−N(bzim), Tables S3, S6, and S12, Supporting Information), which are systematically longer than those found in 1:1 and 1:2 complexes, in line with small bond valences $\nu_{\text{N-ligand}}$ = 0.31−0.32 (Table 1). We can thus safely deduce that the successive connection of ligands to Ln(III) is accompanied by the distortion of the tridentate aromatic unit from planarity and the reduction of its affinity for Ln(III). Since this process results in a stepwise increase of the Ln−N bond lengths, it can be understood as the operation of anticooperative interligand interactions of mainly enthalpic origins. Related calculations using the bond valence method for complexes with terpyridine **L1** (Tables S13−S18, Supporting Information) show no obvious correlation between Ln/**L1** stoichiometry and $\nu_{\text{N-ligand}}$ (Table 5), which restricts the anticooperative effect in the solid state to the specific ligand cavity produced by the connection of two extended benzimidazole rings at the 2 and 6 positions of the central pyridine ring.

If we now turn our attention to the affinity of the additional anions or solvent molecules bound to Ln(III) in 1:1 and 1:2 complexes with **L1**, **L2**, **L2**[a], **L2**[e], and **L2**[f], we obtain the

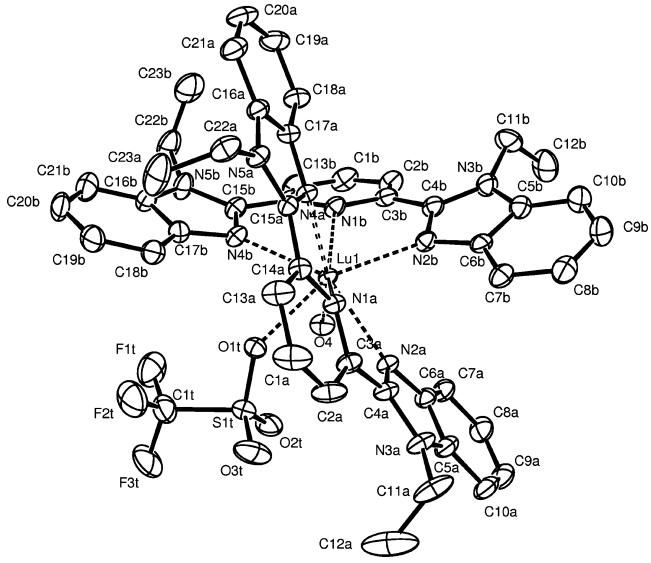

Figure 3. Perspective view of [Lu(**L2**[a])$_2$(Otf)(H$_2$O)]$^{2+}$ in the crystal structure of **3** with numbering scheme. Ellipsoids are represented at the 40% probability level.

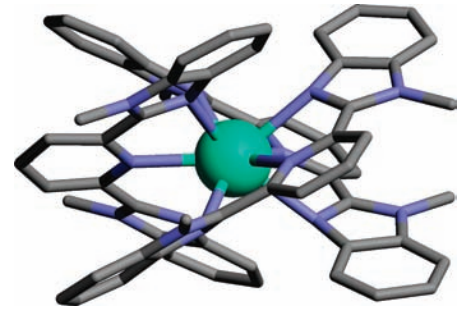

Figure 4. Perspective view of the cation [Eu(**L2**)$_3$]$^{3+}$ in the crystal structure of [Eu(**L2**)$_3$](ClO$_4$)$_3$ highlighting the helical twist of the coordinated ligands. Adapted from ref 11. Copyright 1993. American Chemical Society.

Table 5. Average Bond Valences (v_{ij}, eq 1) and Bond Valence Sums (V_i, eq 2) in the Crystal Structures of 1:1, 1:2, and 1:3 Complexes of **L1** and **L2^k** (X = H) with Trivalent Lanthanides (O-Solv = H_2O or CH_3OH)

complexes	Ln/**L**	$v_{N\text{-ligand}}$	$v_{N\text{-NCS}}$	$v_{O\text{-NO3}}$	$v_{O\text{-CF3CO2}}$	$v_{O\text{-Solv}}$	V_i	ref
[Lu(**L1**)$(NO_3)_3$]	1:1	0.39(1)		0.31(3)			3.04	9
[Lu(**L1**)$(NO_3)_3(CH_3OH)$]	1:1	0.33(1)		0.31(7)		0.39	2.92	9
[La(**L1**)$(NO_3)_4]^-$	1:1	0.28(3)		0.27(2)			3.04	3
[La(**L1**)$_2(NO_3)_2]^+$	1:2	0.32(3)		0.266(7)			3.00	3
[Pr(**L1**)$_2(SCN)_3$]	1:2	0.31(3)	0.42(3)				3.13	49
[Eu(**L1**)$_3]^{3+}$	1:3	0.33(2)					2.95	5
[Lu(**L2^k**)$(NO_3)_3$]	1:1	0.37(4)		0.31(2)			2.96	30
[Lu(**L2^k**)$(CF_3CO_2)_3(H_2O)$]	1:1	0.34(4)			0.40(13)	0.41	3.03	33

following decreasing sequence $v_{O-H2O} \approx v_{O\text{-Otf}} > v_{O\text{-CH3OH}} \approx v_{O\text{-NO3}} > v_{O\text{-ClO4}} > v_{N\text{-CH3CN}}$, which agrees with the classical concept of oxophilicity usually assigned to trivalent lanthanides. Interestingly, we note an exceptional value of $v_{N\text{-NCS}} = 0.42(3)$ for N-bound thiocyanates in [Pr(**L1**)$(SCN)_3$],[49] which does not fit the expected trend. To further support this unique observation, we have reacted $Lu(SCN)_3 \cdot 3H_2O \cdot C_2H_5OH$ with **L2^a** in acetonitrile and observed the successive formation of 1:1 and 2:3 adducts in solution (see next section for stabilities in solution). Crystallization of a concentrated acetonitrile solution containing a Lu/**L2^a** = 1:1 indeed provides X-ray quality prisms of the 2:3 adduct $[Lu_2(\mathbf{L2^a})_3(SCN)_6] \cdot H_2O \cdot 3CH_3CN$ (**4**), whose crystal structure is composed of eight-coordinate $[Lu(\mathbf{L2^a})_2(SCN)_2]^+$ cations and seven-coordinate $[Lu(\mathbf{L2^a})(SCN)_4]^-$ anion in equal amounts, together with interstitial solvent molecules (Figure 5). As expected, (i) the Lu−N bond lengths are shorter in the 1:1 anionic complex (Table 6), which gives $v_{N\text{-ligand}}([Lu(\mathbf{L2^a})(SCN)_4]^-) > v_{N\text{-ligand}}([Lu(\mathbf{L2^a})_2(SCN)_2]^+)$ (Table 1), and (ii) the distortion of the tridentate aromatic ligand is more pronounced in the 1:2 complex (bzim-py interplane angles, 15.7−19.7°, average = 17(3)° for $[Lu(\mathbf{L2^a})(SCN)_4]^-$ and 13.6−37.2°, average = 25(11)° for $[Lu(\mathbf{L2^a})_2(SCN)_2]^+$, Table S25, Supporting Information). We also detect a weak intermolecular aromatic π-stacking interaction involving one benzimidazole ring of $[Lu(\mathbf{L2^a})_2(SCN)_2]^+$ and the benzimidazole-pyridine unit of $[Lu(\mathbf{L2^a})(SCN)_4]^-$ (interplane distance = 3.6 Å, interplane angle = 4.9°), but the overlap is minute. However, $v_{N\text{-NCS}}$ = 0.46−0.53 confirm the strong affinity of N-bound thiocyanates for trivalent lanthanides. The isolation of an unusual 2:3 adduct is reminiscent of the crystallization of $[La(\mathbf{L1})_2(NO_3)_2][La(\mathbf{L1})(NO_3)_4] \cdot 1/2H_2O \cdot CH_3CN$ in an NMR tube containing a large excess of ligand.[3] Finally, we have checked that bulky substituents attached at the 6-positions of the distal benzimidazole rings in **L2^k** do not significantly affect ligand affinity and the organization of the metallic coordination spheres in the 1:1 complexes $[Lu(\mathbf{L2^k})(NO_3)_3]$[30] and $[Lu(\mathbf{L2^k})(CF_3CO_2)_3]$.[33] The bond valence method gives $v_{N\text{-ligand}}$ and $v_{O\text{-anions}}$ (Table S19 and S20, Supporting Information) very similar to those obtained in absence of substituents (Tables 1 and 2), but it is worth noting that the replacement of NO_3^- with more coordinating $CF_3CO_2^-$ anions is accompanied by a slight decrease of $v_{N\text{-ligand}}$, in complete agreement with the improved thermal stability of this complex with nitrate counteranions.[33]

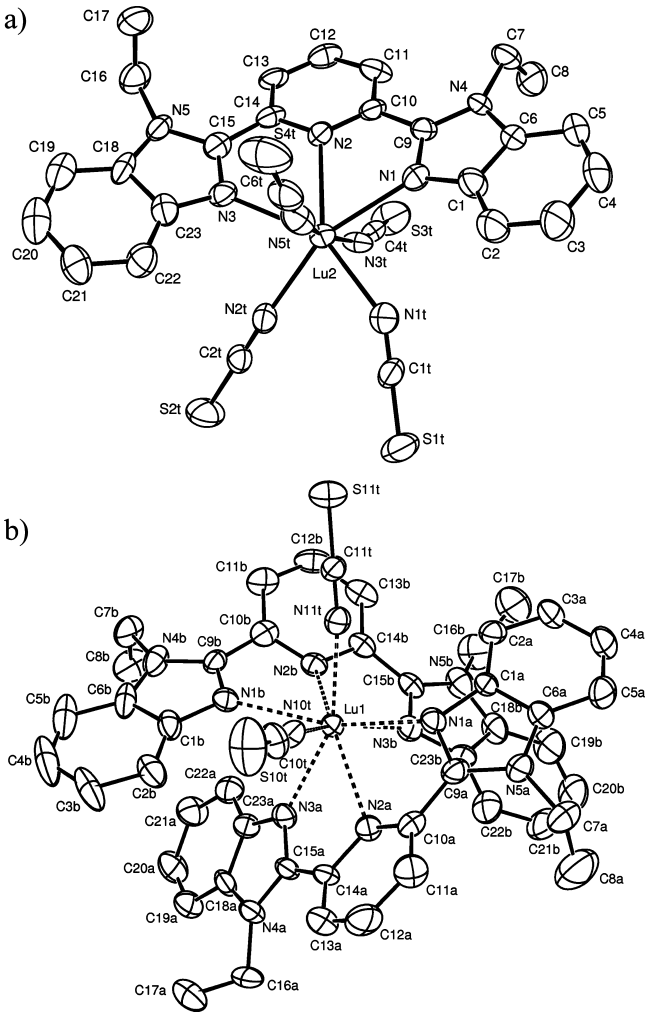

Figure 5. Perspective views of (a) $[Lu(\mathbf{L2a})_2(SCN)_2]^+$ and (b) $[Lu(\mathbf{L2a})(SCN)_4]^-$ in the crystal structure of **4** with numbering scheme. Ellipsoids are represented at the 40% probability level.

Speciation, Stabilities, and Site Binding Analysis in Solution. The thermodynamic formation constants for the purely intermolecular complexation processes described in equilibrium 3 can be easily modeled with the site binding model (eq 4), which considers one combined statistical factor $\omega_{1,m}^{chiral} \cdot \omega_{1,m}^{Ln,L}$ and two microscopic parameters $f_i^{Ln,L}$ and $u_{k,l}^{L,L}$.[41,42,50]

(49) Cotton, S. A.; Franckevicius, V.; How, R. E.; Ahrens, B.; Ooi, L. L.; Mahon, M. F.; Raithby, P. R.; Teat, S. J. *Polyhedron* **2003**, *22*, 1489–1497.

(50) Borkovec, M.; Hamacek, J.; Piguet, C. *Dalton Trans.* **2004**, 4096–4105.

Table 6. Selected Bond Distances (Å) and Angles (deg) for [[Lu(**L2**^{a})(SCN)$_4$][Lu(**L2**^{a})$_2$(SCN)$_2$]·H$_2$O·3CH$_3$CN (**4**)

		bond distances			
Lu1−N1a	2.447(6)	Lu1−N1b	2.447(7)	Lu1−N10t	2.313(7)
Lu1−N3a	2.438(6)	Lu1−N3b	2.443(7)	Lu1−N11t	2.337(7)
Lu1−N2a	2.571(6)	Lu1−N2b	2.531(6)		
Lu2−N1	2.419(7)	Lu2−N2	2.490(6)	Lu2−N3	2.410(7)
Lu2−N1t	2.312(9)	Lu2−N3t	2.280(9)	Lu2−N2t	2.300(7)
Lu2−N5t	2.294(8)				
		N−Lu1−N bite angles			
N1a−Lu1−N2a	64.2(2)	N1a−Lu1−N3a	125.6(2)	N2a−Lu1−N3a	64.2(2)
N1b−Lu1−N2b	64.6(2)	N1b−Lu1−N3b	124.6(2)	N2b−Lu1−N3b	64.1(2)
N1a−Lu1−N1b	155.5(2)	N1a−Lu1−N2b	121.7(2)	N1a−Lu1−N3b	73.8(2)
N2a−Lu1−N1b	123.9(2)	N2a−Lu1−N2b	150.0(2)	N2a−Lu1−N3b	93.3(2)
N3a−Lu1−N1b	73.3(2)	N3a−Lu1−N2b	96.0(2)	N3a−Lu1−N3b	92.9(2)
		N−Lu1−N angles			
N1a−Lu1−N11t	78.3(2)	N3a−Lu1−N11t	155.6(2)	N3a−Lu1−N10t	95.1(2)
N2a−Lu1−N11t	134.9(2)	N2a−Lu1−N10t	69.4(2)	N1a−Lu1−N10t	82.4(2)
N1b−Lu1−N11t	82.3(2)	N1b−Lu1−N10t	80.2(2)	N2b−Lu1−N11t	71.6(2)
N2b−Lu1−N10t	138.0(2)	N3b−Lu1−N11t	99.8(2)	N3b−Lu1−N10t	155.1(2)
N11t−Lu1−N10t	82.1(2)				
		N−Lu2−N bite angles			
N1−Lu2−N2	65.3(2)	N1−Lu2−N3	125.3(2)	N2−Lu2−N3	64.8(2)
		N−Lu2−N angles			
N1−Lu1−N1t	83.3(3)	N1−Lu2−N3t	82.7(2)	N1−Lu2−N2t	157.0(2)
N1−Lu2−N5t	88.0(2)	N2−Lu1−N1t	146.2(3)	N2−Lu2−N3t	73.2(2)
N2−Lu2−N2t	129.2(2)	N2−Lu2−N5t	102.9(3)	N3−Lu2−N1t	149.0(3)
N3−Lu2−N3t	102.9(3)	N3−Lu2−N2t	76.6(2)	N3−Lu2−N5t	82.4(3)
N1t−Lu2−N3t	91.3(3)	N1t−Lu2−N2t	77.4(3)	N1t−Lu2−N5t	87.5(3)
N3t−Lu2−N2t	85.4(3)	N3t−Lu2−N5t	170.7(3)	N2t−Lu2−N5t	103.4(3)

$$\mathrm{Ln}^{3+} + m\mathrm{L} \rightleftharpoons [\mathrm{LnL}_m]^{3+} \qquad \beta_{1,m}^{\mathrm{Ln,L}} \tag{3}$$

$$\beta_{1,m}^{\mathrm{Ln,L}} = \mathrm{e}^{-\Delta G_{1,m}^{\mathrm{Ln,L}}/RT} = \omega_{1,m}^{\mathrm{chiral}} \cdot \omega_{1,m}^{\mathrm{Ln,L}} \cdot \prod_{i=1}^{m} f_i^{\mathrm{Ln,L}} \cdot \prod_{k<l} u_{k,l}^{\mathrm{L,L}} \tag{4}$$

Following Benson's strategy,[51] the geometrical part of the statistical factor $\omega_{1,m}^{\mathrm{Ln,L}}$ can be obtained by using the symmetry number method.[52] Briefly, $\omega_{1,m}^{\mathrm{Ln,L}}$ is given by the ratio between the products of the symmetry numbers, σ_i, of the reactants and that of the product species taken to the power of their stoichiometric coefficients (eq 5).

$$\omega_{1,m}^{\mathrm{Ln,L}} = \prod_i (\sigma_i^{\mathrm{reactant}})^{n_i} \Big/ \prod_j (\sigma_j^{\mathrm{products}})^{n_j} = (\sigma_{\mathrm{L}})^m \cdot \sigma_{\mathrm{Ln}}/\sigma_{\mathrm{LnLm}} \tag{5}$$

Each factor σ is itself the product of external σ^{ext} and internal σ^{int} symmetry numbers: σ^{ext} corresponds to the number of different, but indistinguishable atomic arrangements obtained by rotating a molecule with symmetry operations of the first kind, and σ^{int} refers to the same definition relevant to internal rotations about single bonds within a molecule. When a molecule exists at equilibrium as a racemic mixture, its symmetry number must be divided by two to account for the entropy of mixing of the two enantiomers.[52] This latter effect can be introduced as a correction term given in eq 6.

$$\omega_{1,m}^{\mathrm{chiral}} = \prod_i (\sigma_i^{\mathrm{chiral,reactant}})^{n_i} \Big/ \prod_j (\sigma_j^{\mathrm{chiral,products}})^{n_j} = (\sigma_{\mathrm{L}}^{\mathrm{chiral}})^m \cdot \sigma_{\mathrm{Ln}}^{\mathrm{chiral}}/\sigma_{\mathrm{LnLm}}^{\mathrm{chiral}} \tag{6}$$

Application of this technique leads to the statistical factors calculated in Figure 6 for the formation of 1:1 (eq 7), 1:2 (eq 8), and 1:3 (eq 9) complexes with the tridentate ligand **L2**.

$f_i^{\mathrm{Ln,L}}$ represents the intermolecular microscopic affinity (including desolvation) characterizing the connection of Ln(III) to the multidentate binding site i of **L** and $u_{k,l}^{\mathrm{L,L}} = e^{-(\Delta E_{k,l}^{\mathrm{L,L}}/RT)}$ is the Boltzmann's factor accounting for interligand free energy of interaction $\Delta E_{k,l}^{\mathrm{L,L}}$ operating when two ligands are bound to the same metal.[41,42] Since two parameters $f_i^{\mathrm{Ln,L}}$ and $u_{k,l}^{\mathrm{L,L}}$ should be obtained from the thermodynamic data, a minimum set of three formation constants are required for ensuring a reliable fitting process.

The ^{1}H NMR titration of **L2**^{a} with La(Co(C$_2$H$_{11}$B$_9$)$_2$)$_3$·8H$_2$O·1.6(C$_2$H$_5$)O in CD$_3$CN demonstrates the successive formation of the three 1:1, 1:2, and 1:3 complexes when strictly noncoordinating anions are used in acetonitrile (Figure 7),[53] in agreement with similar results previously reported for the titration of **L2** with Ln(ClO$_4$)$_3$ in the same solvent.[21] Unfortunately, the bulky cobalticarborane Co(C$_2$H$_{11}$B$_9$)$_2^-$ anion strongly absorbs in the UV part of the electronic spectrum, which prevents a reliable monitoring of the moderate absorption changes accompanying the complexation of Ln(III) to **L2**^{a} during the spectrophotometric titrations. Alternatively, the spectrophotometric titrations of **L2**^{a} with LnX$_3$·nH$_2$O (X = ClO$_4^-$, Otf$^-$), which contain nonabsorbing and noncoordinating counteranions, indeed confirm the successive formation of three absorbing complexes in acetonitrile characterized by smooth end points at Ln/**L2**^{a} = 1:3, Ln/**L2**^{a} = 1:2, and Ln/**L2**^{a} = 1:1 (Figure 8a and b). A comparison with original data previously collected for **L2** titrated with Ln(ClO$_4$)$_3$·nH$_2$O (Figure 8c)[11,21] shows considerable similarities, and each set of spectrophotometric data can be satisfyingly fitted to eq 7−9 with the macroscopic formation constants collected in Table 7.

(51) Benson, S. W. *J. Am. Chem. Soc.* **1958**, *80*, 5151–5154.
(52) Ercolani, G.; Piguet, C.; Borkovec, M.; Hamacek, J. *J. Phys. Chem. B* **2007**, *111*, 12195–12203.
(53) Long, D.-L.; Blake, A. J.; Champness, N. R.; Wilson, C.; Schröder, M. *Angew. Chem., Int. Ed.* **2001**, *40*, 2444–2447.

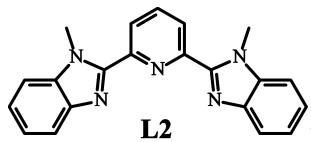

$$\mathbf{L2} + [Ln(CH_3CN)_9]^{3+} \overset{\beta_{1,1}^{Ln,L2}}{\rightleftharpoons} [Ln(CH_3CN)_6(\mathbf{L2})]^{3+} + 3\,CH_3CN \quad (7)$$

Point groups:	C_{2v}	D_{3h}	C_{2v}	C_{3v}
σ^{ext}:	2	6	2	3
σ^{int}:	3^2	3^9	$3^2 \cdot 3^6$	1
σ^{chiral}:	1	1	1	1

$$\Rightarrow \omega_{1,1}^{chiral} = \frac{1 \cdot 1}{1 \cdot 1} = 1 \qquad \omega_{1,1}^{Ln,L2} = \frac{2 \cdot 3^2 \cdot 6 \cdot 3^9}{2 \cdot 3^2 \cdot 3^6 \cdot 3^3} = 6$$

$$2\,\mathbf{L2} + [Ln(CH_3CN)_9]^{3+} \overset{\beta_{1,2}^{Ln,L2}}{\rightleftharpoons} [Ln(CH_3CN)_3(\mathbf{L2})_2]^{3+} + 6\,CH_3CN \quad (8)$$

Point groups:	C_{2v}	D_{3h}	C_{2v}	C_{3v}
σ^{ext}:	2	6	2	3
σ^{int}:	3^2	3^9	$3^4 \cdot 3^3$	1
σ^{chiral}:	1	1	1	1

$$\Rightarrow \omega_{1,2}^{chiral} = \frac{1 \cdot 1}{1 \cdot 1} = 1 \qquad \omega_{1,2}^{Ln,L2} = \frac{\left(2 \cdot 3^2\right)^2 \cdot 6 \cdot 3^9}{2 \cdot 3^4 \cdot 3^3 \cdot 3^6} = 12$$

$$3\,\mathbf{L2} + [Ln(CH_3CN)_9]^{3+} \overset{\beta_{1,3}^{Ln,L2}}{\rightleftharpoons} [Ln(\mathbf{L2})_3]^{3+} + 9\,CH_3CN \quad (9)$$

Point groups:	C_{2v}	D_{3h}	D_3	C_{3v}
σ^{ext}:	2	6	6	3
σ^{int}:	3^2	3^9	3^6	1
σ^{chiral}:	1	1	1/2	1

$$\Rightarrow \omega_{1,3}^{chiral} = \frac{1 \cdot 1}{1 \cdot 1/2} = 2 \qquad \omega_{1,3}^{Ln,L2} = \frac{\left(2 \cdot 3^2\right)^3 \cdot 6 \cdot 3^9}{6 \cdot 3^6 \cdot 3^9} = 8$$

Figure 6. Statistical factors for the successive fixation of three tridentate aromatic ligands to nine-coordinate Ln(III).

The application of the site binding model (eq 4) to each set of cumulative formation constants (eqs 7−9) provides three equations for each lanthanide (eqs 10−12, statistical factors taken from Figure 6) for fitting two parameters $f_{N3}^{Ln,L}$ and $u^{L,L}$, respectively measuring the absolute affinity of the tridentate 2,6-bis(benzimidazol-2-yl)pyridine units in **L2** or **L2**[a] for Ln(III) (including desolvation) and the interligand interactions resulting from the coordination of two N_3 binding unit to the central metal (Table 8).

$$\beta_{1,1}^{Ln,L} = 6 \cdot f_{N3}^{Ln,L} \quad (10)$$

$$\beta_{1,2}^{Ln,L} = 12 \cdot (f_{N3}^{Ln,L})^2 \cdot u^{L,L} \quad (11)$$

$$\beta_{1,3}^{Ln,L} = 16 \cdot (f_{N3}^{Ln,L})^3 \cdot (u^{L,L})^3 \quad (12)$$

As previously established when measuring the third successive stability constant leading to $[Ln(\mathbf{L2})_3]^{3+}$,[21] we observe a maximum affinity $f_{N3}^{Ln,L}$ of the N_3 binding units in **L2** and **L2**[a] for midrange Ln(III). Interestingly, the interligand interactions are systematically repulsive ($1.5 < \Delta E^{L,L} < 9$ kJ/mol, anticooperative processes), which disfavors the successive binding of ligands to the same metallic center, as similarly found with the analogous terpyridine ligand in acetonitrile (entries 1−3 in Table 8). We however do not detect significant variations of these microscopic parameters on going from **L2** to **L2**[a] or on replacing ClO_4^- with Otf^- (Table 8). The same approach applied to the more bulky ligands $\mathbf{L}^{o-q}$ (chart 3), indeed shows the formation of less stable 1:1 and 1:2 complexes characterized by smaller microscopic affinities $f_{N3}^{Ln,L}$, which can be partly assigned to the use of a more competiting solvent for solubility reasons (CH_2Cl_2/CH_3CN = 1:1, Table 9). However, the interligand interactions are systematically larger ($10 < \Delta E^{L,L} < 12$ kJ/mol), which severely limits the successive coordination of additional bulky ligands to Ln(III). Taking the microscopic parameters collected in Table 9, we calculate with eq 12 that $\log (\beta_{1,3}^{Ln,L})_{calcd} = 11-12$ for the 1:3 complexes with the bulky ligands $\mathbf{L}^{o-q}$, a low value which explains the nondetection of this species during spectrophotometric titrations. These results illustrate how minor changes in interligand interactions may tune the output of the complexation process.

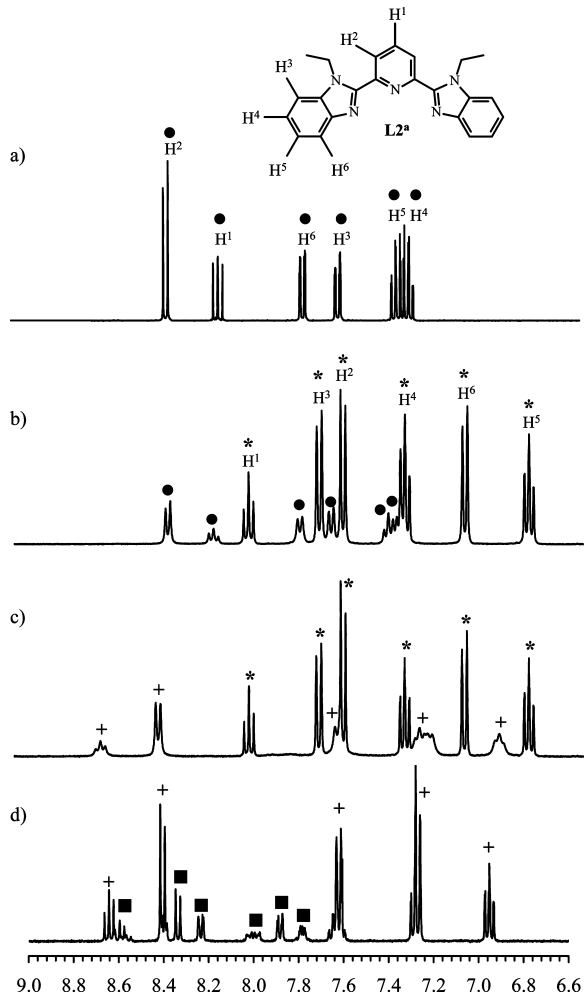

Figure 7. Aromatic part of the ^{1}H NMR titration of **L2^a** with $La(Co(C_2H_{11}B_9)_2)_3$ in CD_3CN for (a) La/**L2^a** = 0:1, (b) La/**L2^a** = 1:3.5, (c) La/**L2^a** = 1:2.3, and (d) La/**L2^a** = 1:1.2 (● = **L2^a**, ∗ = $[La(\mathbf{L2^a})_3]^{3+}$, + = $[La(\mathbf{L2^a})_2]^{3+}$, and ■ = $[La(\mathbf{L2^a})]^{3+}$).

When the spectrophotometric titrations of **L2^a** are performed with lanthanide salts LnX_3 containing more coordinating counteranions (X = Cl^-, NO_3^-, SCN^-, Figure 9), the formation of 1:1 complexes dominates the speciation, together with some other adducts with 1:2, 1:3, or 2:3 stoichiometries (Table 7). Detailed ^{1}H NMR studies show the formation of intricate mixtures of slowly (on the NMR time scale) interconverting complexes, in line with the very complicated speciation previously established for the titration of **L1** with $La(NO_3)_3$, for which seven different complexes could be evidenced.[3] We however note that $\log(\beta_{1,1}^{Ln,L})$ decreases in the order X = $ClO_4^- \approx Otf^- > NO_3^- \approx SCN^- > Cl^-$, but the titrations with chloride anions have been performed in propylene carbonate for solubility reasons, which limits the comparisons.

In this context, we have selected the titration of the lipophilic and highly soluble hexacatenar tridentate ligand **L2^q** (Chart 3) with $Eu(NO_3)_3 \cdot 3H_2O$ as a study case for highlighting the importance of minor solvent changes on the stability and speciation of these complexes in solution. Previous work on $[Eu(\mathbf{L2^q})(NO_3)_3]$ in CD_2Cl_2 by using variable-temperature NMR (VT-NMR) combined with diffusion-ordered NMR (DOSY-NMR) firmly established that this complex exists in equilibrium with its nitrato-bridged dimer (eq 13) and that dissociation of the tridentate ligand is negligible at 10 mM concentration.[30]

$$2[Eu(\mathbf{L2^q})(NO_3)_3] \rightleftharpoons [Eu_2(\mathbf{L2^q})_2(NO_3)_6] \quad K_{dim}^{Eu,L2q} \quad (13)$$

The repetition of these NMR measurements for the same complex, but in $CDCl_3$, leads to very similar conclusions with the coexistence of monomer and dimer as the main complex species in solution at 10 mM concentration (Figure S4, Supporting Information) with autodiffusion coefficients ($D_{monomer}^{298K} = 3.74(4) \cdot 10^{-10}$ m^2s^{-1} and $D_{dimer}^{298K} = 2.82(3) \cdot 10^{-10}$ m^2s^{-1}), whose ratio $D_{monomer}^{298K}/D_{dimer}^{298K} = 1.32(1)$ fairly matches $2^{1/3} = 1.26$ expected for the diffusion of two pseudospherical species possessing identical molecular densities, but with molecular weights in the 1:2 ratio.[54] We however detect significant decomplexation of the tridentate ligand in $CDCl_3$ as a result of the reduction of the formation constants of the monomeric and dimeric complexes in this solvent. At low temperature (233−268 K), the variable-temperature NMR spectra collected for Eu/**L2^q** = 1.0 in $CDCl_3$ show broad signals typical for intermediate exchange on the NMR time scale, and which point to the existence of three different ligand environments assigned to **L2^q**, $[Eu(\mathbf{L2^q})(NO_3)_3]$ and $[Eu_2(\mathbf{L2^q})_2(NO_3)_6]$ (Figure S4, Supporting Information). Integration of these VT-NMR data after deconvolution allows the estimation of $\beta_{1,1}^{Eu,L2q}$, $\beta_{2,2}^{Eu,L2q}$, and $K_{dim}^{Eu,L2q} = \beta_{2,2}^{Eu,L2q}/(\beta_{1,1}^{Eu,L2q})^2$ at each temperature (Table S26, Supporting Information), from which the enthalpic and entropic contributions to the dimerization process can be evaluated by using van't Hoff plots (eq 14, Figure 10). At higher temperature ($T > 270$ K), a close scrutiny at the spectra show the appearance of a fourth species in low concentration (probably a partially solvated species as reported for $[La(\mathbf{L1})(NO_3)_3]$),[3] which prevents a simple analysis of the speciation using eq 13 (Figure S4, Supporting Information).

$$-R \ln(K_{dim}^{Eu,L2q}) = \Delta H_{dim}^{Eu,L2q}/T - \Delta S_{dim}^{Eu,L2q} \quad (14)$$

As previously found in CD_2Cl_2 ($\Delta H_{dim}^{Eu,L2q} = -25(2)$ kJ/mol and $\Delta S_{dim}^{Eu,L2q} = -47(5)$ J/mol^{-1} K^{-1}),[30] both enthalpic and entropic contributions to the dimerization processes are still negative in $CDCl_3$ ($\Delta H_{dim}^{Eu,L2q} = -5(2)$ kJ/mol and $\Delta S_{dim}^{Eu,L2q} = -1(10)$ J mol^{-1} K^{-1}), which is diagnostic for the formation of the nitrato bridge in the dimer as the dominant factor of the thermodynamic process. However, their drastic reduction in magnitude in $CDCl_3$ implies a much larger contribution of the desolvation of the reactants.[55,56] Moreover, the additional van't Hoff plots of $-R \ln(\beta_{1,1}^{Eu,L2q})$ versus T^{-1} (Figure S5a, Supporting Information) and $-R \ln(\beta_{2,2}^{Eu,L2q})$ versus T^{-1} (Figure S5b, Supporting Information) provides unfavorable positive enthalpies of complexation $\Delta H_{1,1}^{Eu,L2q} = 13(4)$ kJ/mol and $\Delta H_{2,2}^{Eu,L2q} = 21(6)$ kJ/mol, balanced by highly positive entropies $\Delta S_{1,1}^{Eu,L2q} = 109(15)$ J mol^{-1} K^{-1} and $\Delta S_{2,2}^{Eu,L2q} = 218(26)$ J mol^{-1} K^{-1}, which ensures the

(54) Greenwald, M.; Wessely, D.; Goldberg, I.; Cohen, Y. *New J. Chem.* **1999**, *33*, 7–344.
(55) Motekaitis, R. J.; Martell, A. E.; Hancock, R. A. *Coord. Chem. Rev.* **1994**, *133*, 39–65.
(56) Piguet, C.; Bünzli, J.-C. G. *Chem. Soc. Rev.* **1999**, *28*, 347–358.

stability of the final complexes and are diagnostic for a complexation process controlled by the desolvation steps in $CDCl_3$.[55,56] Finally, the recurrent observation of the unusual 2:3 stoichiometry for titrations of either $Ln(NO_3)_3$ or $Ln(SCN)_3$ with **L2**[a] in solution (Table 7), which is substantiated by the crystal structures obtained for $[La(\mathbf{L1})_2(NO_3)_2]$-$[La(\mathbf{L1})(NO_3)_4]$[3] and $[Lu(\mathbf{L2}^a)_2(SCN)_2][Lu(\mathbf{L2}^a)(SCN)_4]$ (**4**), can be understood as the result of the transfer of one coordinated anion in a mixture of 1:1 and 1:2 complexes in solution according to equilibrium 15.

$$[Ln(\mathbf{L2})X_3] + [Ln(\mathbf{L2})_2X_3] \rightleftharpoons [Ln(\mathbf{L2})X_4]^- + [Ln(\mathbf{L2})_2X_2]^+ \quad K_{exch}^{Ln,X} \quad (15)$$

The exchange constant $K_{exch}^{Ln,X}$ is given by the ratio of the pair products of the cumulative formation constants in eq 16, each of them being easily modeled by using the site binding model (eq 4, Figure S6, Supporting Information). Substitution into eq 16 eventually shows that $K_{exch}^{Ln,X}$ only depends on the interligand Boltzmann's factors: $u^{L,X} = e^{-\Delta E^{L,X}/RT}$ standing for anion−**L2** interactions and $u^{X,X} = e^{-\Delta E^{X,X}/RT}$ standing for anion−anion interactions.

$$K_{exch}^{Ln,X} = \frac{\beta_{1,1,4}^{Ln,L2,X} \cdot \beta_{1,2,2}^{Ln,L2,X}}{\beta_{1,1,3}^{Ln,L2,X} \cdot \beta_{1,2,3}^{Ln,L2,X}} = \frac{u^{X,X}}{(u^{L,X})^3} \quad (16)$$

Application of the Gibbs relationship gives $\Delta G_{exch}^{Ln,X} = 3\Delta E^{L,X} - \Delta E^{X,X}$, which allows a simple interpretation of the driving force for the anion transfer described in reaction 15. Assuming the operation of usual repulsive interligand interactions, that is, $\Delta E^{L,X} > 0$ and $\Delta E^{X,X} > 0$, we deduce that $\Delta G_{exch}^{Ln,X}$ is favorable, that is, negative, when the interanion repulsion dominates, a situation encountered for anions closely bound to the metallic center. According to the solid-state structure and the bond valence values, the thiocyanate anions display the closest interactions with Ln(III), followed

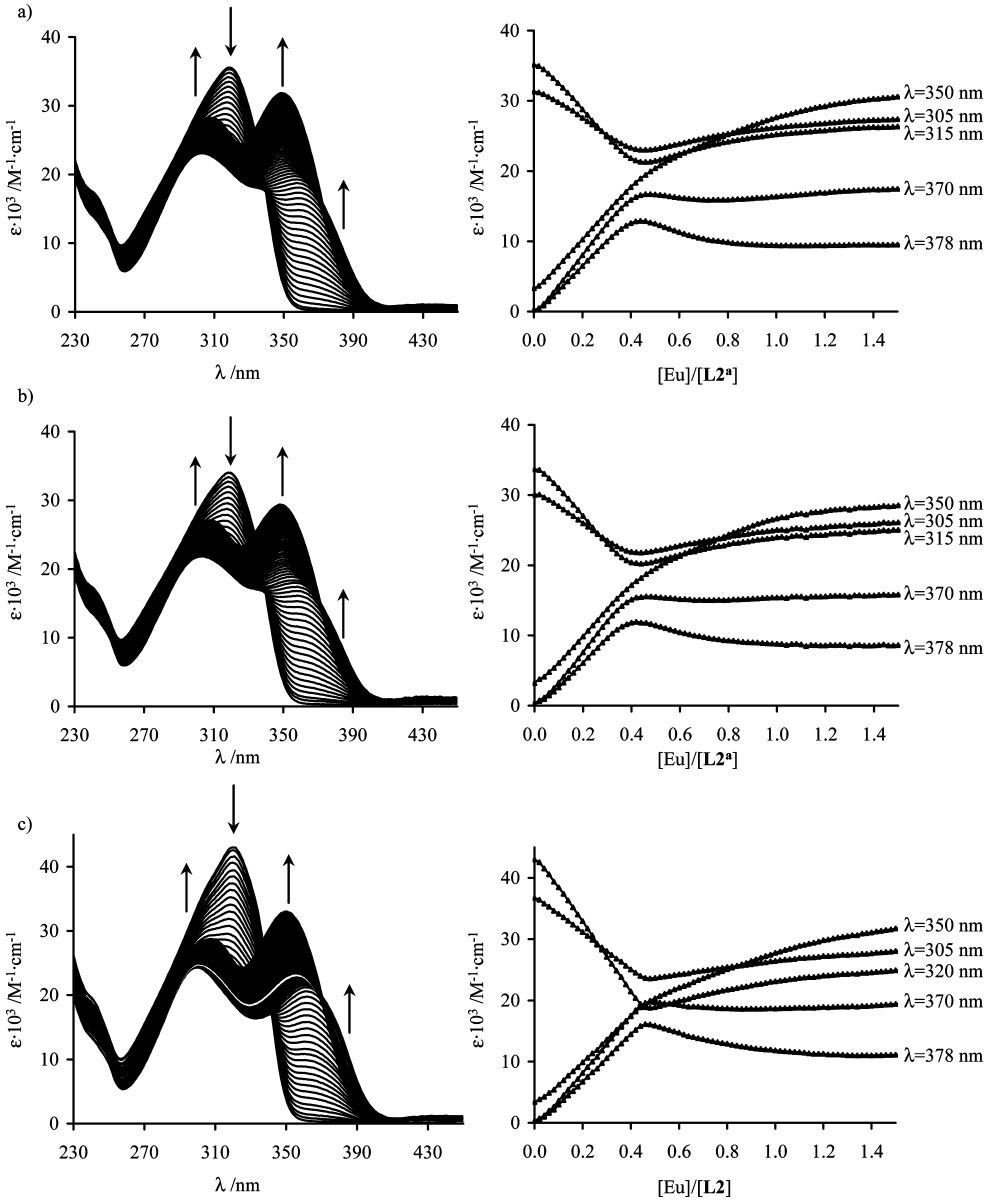

Figure 8. Variation of absorption spectra and corresponding variation of observed molar extinctions at 5 different wavelengths observed for the spectrophotometric titrations of (a) **L2**[a] with $Eu(ClO_4)_3 \cdot 7H_2O$, (b) **L2**[a] with $Eu(Otf)_3 \cdot 3H_2O$, and (c) **L2** with $Eu(ClO_4)_3 \cdot 7H_2O$ (2×10^{-4} mol dm^{-3} in acetonitrile, 298 K).

Table 7. Selected Thermodynamic Formation Constants Obtained from Spectrophotometric Titrations of **L2** and **L2**[a] with $LnX_3 \cdot nH_2O$ in Solution (298 K)

ligand	Ln(III)	Anion	Solvent	$\log(\beta_{1,1}^{Ln,L})$	$\log(\beta_{1,2}^{Ln,L})$	$\log(\beta_{1,3}^{Ln,L})$	$\log(\beta_{2,3}^{Ln,L})$
L2	Eu	ClO_4^-	CH_3CN	7.7(4)	15.1(6)	20.5(1)	
L2	Y	ClO_4^-	CH_3CN	7.8(1)	13.9(2)	19.5(2)	
L2[a]	La	ClO_4^-	CH_3CN	6.4(2)	12.2(2)	17.4(3)	
L2[a]	Eu	ClO_4^-	CH_3CN	7.8(4)	15.1(6)	21.1(7)	
L2[a]	Er	ClO_4^-	CH_3CN	7.0(2)	13.7(2)	18.0(2)	
L2[a]	Lu	ClO_4^-	CH_3CN	6.8(2)	12.7(4)	16.4(6)	
L2[a]	La	Otf^-	CH_3CN	6.7(2)	12.1(2)	16.5(3)	
L2[a]	Eu	Otf^-	CH_3CN	8.1(3)	15.2(4)	21.2(5)	
L2[a]	Er	Otf^-	CH_3CN	8.6(3)	16.1(5)	20.6(6)	
L2[a]	Lu	Otf^-	CH_3CN	8.1(2)	14.6(2)	[a]	
L2[a]	La	NO_3^-	CH_3CN	4.98(8)		14.3(1)	19.3(1)
L2[a]	Eu	NO_3^-	CH_3CN	4.71(5)	8.6(1)		
L2[a]	Gd	NO_3^-	CH_3CN	4.90(6)	9.0(1)		
L2[a]	Lu	NO_3^-	CH_3CN	6.40(9)			
L2[a]	La	Cl^-	PC[b]	3.06(7)			
L2[a]	Eu	Cl^-	PC[b]	3.89(2)			
L2[a]	Y	SCN^-	CH_3CN	5.46(9)			18.6(3)
L2[a]	Lu	SCN^-	CH_3CN	5.15(3)			18.3(1)

[a] $\log(K_3^{Lu,L})$ is too weak to be determined in these conditions. [b] Propylene carbonate = 4-methyl-1,3-dioxolan-2-one.

Table 8. Fitted Microscopic Thermodynamic Parameters for $[Ln(\mathbf{Lk})_n]^{3+}$ (k = 1, 2, Acetonitrile, 298 K)[a]

ligand	Ln(III)	anion	$\log(f_{N3}^{Ln,L})$	$\Delta G_{con,N3}^{Ln,L}$ (kJ/mol)	$\log(u^{L,L})$	$\Delta E^{L,L}$ (kJ/mol)
L1	La[b]	ClO_4^-	6.8(1)	−38.9(6)	−1.1(1)	6.5(7)
L1	Eu[b]	ClO_4^-	6.9(3)	−39(2)	−1.2(3)	6(2)
L1	Lu[b]	ClO_4^-	7.0(3)	−40(2)	−0.7(4)	4(2)
L2	Eu	ClO_4^-	7.2(3)	−41(2)	−0.8(4)	4(2)
L2	Y	ClO_4^-	6.9(1)	−39.2(8)	−0.8(2)	4(1)
L2[a]	La	ClO_4^-	5.7(1)	−32.3(3)	−0.3(1)	1.5(3)
L2[a]	Eu	ClO_4^-	7.2(2)	−41(1)	−0.5(2)	3(1)
L2[a]	Er	ClO_4^-	6.6(4)	−38(2)	−1.0(5)	5(3)
L2[a]	Lu	ClO_4^-	6.3(3)	−36(1)	−1.2(3)	7(2)
L2[a]	La	Otf^-	5.92(1)	−33.7(1)	−0.823(1)	4.69(1)
L2[a]	Eu	Otf^-	7.39(7)	−42.1(4)	−0.71(8)	4.0(4)
L2[a]	Er	Otf^-	8.2(4)	−46(2)	−1.6(4)	9(2)
L2[a]	Lu	Otf^-	7.3[c]	−42[c]	−1.1[c]	6[c]

[a] The uncertainties correspond to those obtained during the multilinear least-squares fit of eqs 10−12. [b] Cumulative formation constants in acetonitrile +0.1 M Et_4NClO_4 are taken from ref 7. [c] When only two stability constants are available, there is no uncertainties for the fitting of two eqs 10 and 11 with two parameters.

Chart 3

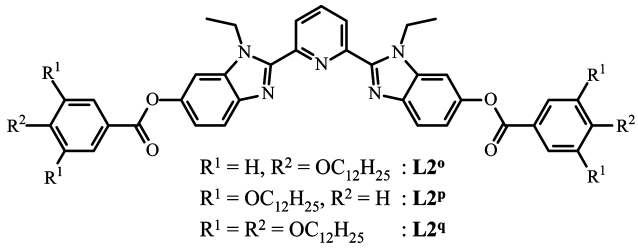

Table 9. Selected Thermodynamic Formation Constants Obtained from Spectrophotometric Titrations of **L2**^{o}, **L2**^{p}, and **L2**^{q} with $Eu(Otf)_3 \cdot 3H_2O$ in Acetonitrile:Dichloromethane (1:1) and Fitted Microscopic Thermodynamic Parameters (298 K)[a]

ligand	$\log(\beta_{1,1}^{Eu,L})$	$\log(\beta_{1,2}^{Eu,L})$	$\log(f_{N3}^{Eu,L})$	$\Delta G_{con,N3}^{Eu,L}$ (kJ/mol)	$\log(u^{L,L})$	$\Delta E^{L,L}$ (kJ/mol)
L2^o	6.2(2)	9.8(6)	5.4	−31	−2.1	12
L2^p	6.1(1)	9.85(3)	5.3	−30	−1.9	11
L2^q	6.3(2)	10.3(5)	5.5	−32	−1.8	10

[a] When only two stability constants are available, there are no uncertainties for the fitting of two eqs 10 and 11 with two parameters.

by NO_3^-, while Cl^- do not interact in the first coordination sphere. This order exactly matches the systematic detection of 2:3 complexes in solution for X = SCN^-, its occasional observation for X = NO_3^-, and its absence for X = Cl^- (Table 7). Since the formation constants $\beta_{1,1,4}^{Ln,L2,X}$ and $\beta_{1,1,2}^{Ln,L2,X}$ are not experimentally accessible by using spectrophotometric titrations, no quantitative data can be currently obtained.

Experimental Section

Chemicals were purchased from Fluka AG and Aldrich and were used without further purification unless otherwise stated. The ligands **L2**,[10] **L2**^{a},[11] **L2**^{h},[30] and **L2**^{q}[30] were prepared according to literature procedures. $Ln(ClO_4)_3 \cdot xH_2O$, $Ln(CF_3SO_3)_3 \cdot xH_2O$, and $Ln(NO_3)_3 \cdot xH_2O$, (Ln = La−Lu) were prepared from the corresponding oxides (Aldrich, 99.99%).[57] $Ln(NCS)_3 \cdot xH_2O \cdot yC_2H_5OH$ (Ln = La−Lu)[49] and $Ln(Co(C_2H_{11}B_9)_2)_3 \cdot xH_2O$ (Ln = La−Lu)[53] were obtained by methathesis from $LnCl_3 \cdot 6H_2O$ by using KSCN and $NaCo(C_2H_{11}B_9)_2$, respectively, according to literature procedures. The Ln content of solid salts was determined by complexometric titrations with Titriplex III (Merck) in the presence of urotropine and xylene orange.[58] Acetonitrile and dichloromethane were distilled over calcium hydride.

***Caution*!** *Dry perchlorates may explode and should be handled in small quantities and with the necessary precautions.*[59,60]

Preparation of 2,6-Bis-[1-ethyl-6-(4-dodecyloxy)-benzoate)-benzimidazol-2-yl]pyridine (L2^o). A catalytic amount of 4-dimethylaminopyridine, 2,6-bis-(1-ethyl-6-hydroxy-benzimidazol-2-yl)pyridine (0.76 g, 1.9 mmol),[30] 4-dodecyloxy-benzoic acid (1.7 g, 5.5 mmol), and 1-(3-dimethylaminopropyl)-3-ethyl-carbodiimide hydrochloride (EDCI, 1.09 g, 5.7 mmol) were refluxed for 2 d in CH_2Cl_2/DMF (190:6 mL). The resulting mixture was washed with half-saturated aq $NaHCO_3$ (50 mL); the organic layer was separated, and the aqueous phase was further extracted with CH_2Cl_2 (3 × 100 mL). The combined organic phase was dried (Na_2SO_4) and evaporated to dryness. The crude residue was purified by column chromatography (silicagel; CH_2Cl_2/MeOH 99:1 → 97:3) to give 1.64 g (1.68 mmol, yield 89%) of **L2**^{o} as a white solid. ^1H NMR in $CDCl_3$: δ_H 0.86−0.89 (6H, t, ^3J = 7 Hz); 1.25−1.34 (32H, m); 1.34−1.38 (6H, t); 1.44−1.56 (4H, m); 1.79−1.86 (4H, m);

(57) Desreux, J. F. In *Lanthanide Probes in Life, Chemical and Earth Sciences*; Bünzli, J.-C. G., Choppin, G. R., Eds.; Elsevier: Amsterdam, 1989; Chapter 2.
(58) Schwarzenbach, G. *Complexometric Titrations*; Chapman & Hall: London, 1957; p. 8.
(59) Wolsey, W. C. *J. Chem. Educ.* **1973**, *50*, A335−A337.
(60) Raymond, K. N. *Chem. Eng. News* **1983**, *61*, 4.

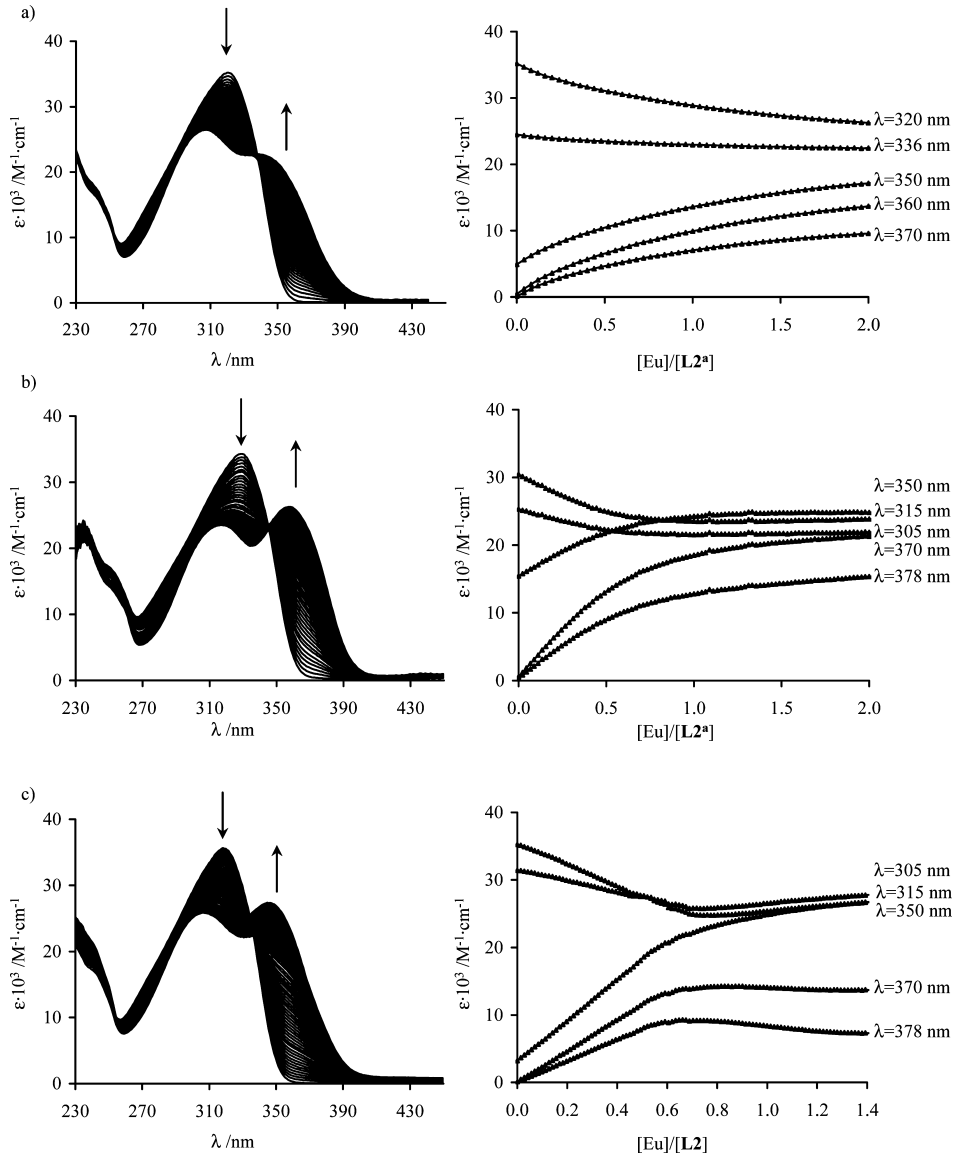

Figure 9. Variation of absorption spectra and corresponding variation of observed molar extinctions at 5 different wavelengths observed for the spectrophotometric titrations of **L2ᵃ** with (a) $EuCl_3 \cdot 6H_2O$ (2×10^{-4} mol dm^{-3} in propylene carbonate, 298 K), (b) $Eu(NO_3)_3 \cdot 3H_2O$, and (c) $Eu(SCN)_3 \cdot 3H_2O \cdot C_2H_5OH$ (2×10^{-4} mol dm^{-3} in acetonitrile, 298 K).

4.03−4.07 (4H, q, $^3J = 7$ Hz); 4.75−4.81 (4H, q, 7 Hz); 6.97−7.01 (4H, m, $^3J = 8.8$. Hz); 7.17−7.19 (2H, dd, $^3J = 8.6$ Hz, $^4J = 2$ Hz); 7.38 (2H, d, $^4J = 2$ Hz); 7.87−7.89 (2H, d, $^3J = 8.6$ Hz); 8.06−8.10 (1H, t, $^3J = 7.8$ Hz); 8.16−8.20 (4H, m, $^3J = 8.8$ Hz); 8.35−8.37 (2H, d,$^3J = 7.8$ Hz). ^{13}C NMR in $CDCl_3$: δ_C 13.94, 15.16 (C_{prim}); 22.49, 25.78, 28.90, 29.14, 29.17, 29.36, 29.39, 29.44, 29.45, 3170, 39.83, 68.01 (C_{sec}); 99.76, 103.46, 114.08, 117.25, 120.54 125.33, 132.04, 135.91 (C_{tert}); 121.38, 140.45, 147.45, 149.58, 150.30, 152.68, 163.33, 165.06 (C_{quat}). ESI-MS (CH_2Cl_2): $m/z = 976.7$ ($[M + H]^+$).

Preparation of 3,5-Di(dodecyloxy)-benzoic Acid. 3,5-Dihydroxybenzoate (4 g, 23.8 mmol) and potassium carbonate (19.7 g, 0.14 mol) were refluxed in dry acetone for 1 h. After addition of 1-bromododecane (23 mL, 95.2 mmol) and a catalytic amount of KI, the white suspension was further refluxed for 2 d. Filtration followed by drying under vacuum produced a white powder, which was dissolved in ethanol/water (150:20 mL) containing potassium hydroxyde (5.33 g, 95.2 mmol). The solution was refluxed for 18 h, poured onto water (100 mL), and neutralized with concentrated aq hydrochloric acid (37%) until pH 1. Ethanol was distilled, and the aqueous phase was extracted with dichloromethane (3×50 mL). The organic layer was evaporated and provided a colorless oil, which slowly crystallized from ethanol at −20 °C to give 9.1 g (18.5 mmol, yield 78%) of white crystals of 3,5-di(dodecyloxy)-benzoic acid. ^{1}H NMR in $CDCl_3$: δ_H 0.85−0.89 (6H, t, $^3J = 7$ Hz); 1.25−1.34 (32H, m); 1.40−1.47 (4H, m); 1.72−1.79 (4H, m); 3.94−3.97 (4H, t, $^3J = 7$ Hz); 6.62−6.63 (1H, t, $^4J = 2$ Hz); 7.14−7.15 (2H, d, $^4J = 2$ Hz). ESI-MS (CH_2Cl_2): $m/z = 489.9$ ($[M - H]^-$).

Preparation of 2,6-Bis-[1-ethyl-6-(4-dodecyloxy)-benzoate)-benzimidazol-2-yl]pyridine (L2ᵖ). The same procedure described for **L2ᵒ** was followed for **L2ᵖ** (yield 51%), except for the replacement of 4-dodecyloxy-benzoic acid with 3,5-di(dodecyloxy)-benzoic acid. ^{1}H NMR in $CDCl_3$: δ_H 0,85−0.88 (12H, t, $^3J = 7$ Hz); 1.25−1.33 (64H, m); 1.34−1.38 (6H, t); 1.44−1.56 (8H, m); 1.76−1.83 (8H, m); 3.99−4.03 (8H, q, $^3J = 7$ Hz); 4.75−4.81 (4H, q, 7 Hz); 6.72−6.73 (2H, t, $^4J = 2.5$ Hz); 7.16−7.19 (2H, dd, $^3J = 8.8$ Hz, $^4J = 2$ Hz); 7.35−7.36 (4H, d, $^4J = 2.5$ Hz); 7.37−7.38 (2H, d, $^4J = 2$. Hz); 7.87−7.89 (2H, d, $^3J = 8.8$ Hz); 8.05−8.09 (1H, t, $^3J = 7.8$ Hz); 8.34−8.36 (2H, d,$^3J = 7.8$ Hz). ^{13}C NMR in

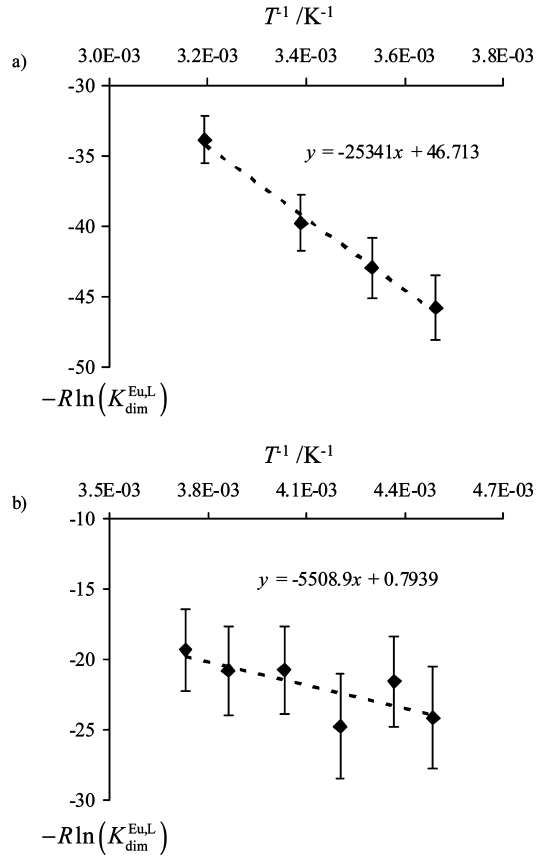

Figure 10. van't Hoff plots for equilibrium 13 in (a) CD_2Cl_2[33] and (b) $CDCl_3$.

$CDCl_3$: δ_C 14.14, 15.42 (C_{prim}); 22.27, 26.08, 29.22, 29.36, 29.40, 29.58, 29.60, 29.65, 29.71, 30.07, 39.98, 68.55 (C_{sec}); 103.60, 107.11, 108.29, 117.40, 120.70, 125.59, 131.28, 138.14 (C_{tert}); 100.02, 131.28, 136.11, 140.71, 147.61, 149.67, 150.69, 160.23, 165.44 (C_{quat}). ESI-MS (CH_2Cl_2): m/z = 1345.4 ($[M + H]^+$).

Preparation of the Complexes $[Lu(L2^h)(H_2O)_5]Cl_3\cdot CH_3NO_2$ (1), $[Lu(L2^a)(Otf)_3(CH_3CN)(H_2O)]$ (2), $[Lu(L2^a)_2(Otf)(H_2O)](Otf)_2$ (3), and $[Lu_2(L2^a)_3(SCN)_6]\cdot H_2O\cdot 3CH_3CN$ (4). Stoichiometric amounts of the ligand and of the target Lu(III) salts were reacted in acetonitrile/dichloromethane (1:1) at rt for one hour (acetonitrile was replaced with propylene carbonate for the chloride salts for solubility reasons). Evaporation to dryness followed by slow diffusion of diisopropyl ether in concentrated solutions of the complexes in acetonitrile (nitromethane for **1**) gave X-ray quality crystals of **1**−**4**.

Single Crystal Structure Determinations of $Lu(L2^h)(H_2O)_5]Cl_3\cdot CH_3NO_2$ (1), $[Lu(L2^a)(Otf)_3(CH_3CN)(H_2O)]$ (2), $[Lu(L2^a)_2(Otf)(H_2O)](Otf)_2$ (3), and $[Lu_2(L2^a)_3(SCN)_6]\cdot H_2O\cdot 3CH_3CN$ (4). Summary of crystal data, intensity measurements, and structure refinements are collected in Table 10. All crystals were mounted on quartz fibers with protection oil. Cell dimensions and intensities were measured at 200 (**1** and **2**) or 220 K (**3** and **4**) on a Stoe IPDS diffractometer with graphite-monochromated Mo[Kα] radiation (λ = 0.71073 Å). Data were corrected for Lorentz and polarization effects and for absorption. The structures were solved by direct methods (SIR97);[61] all other calculation were performed with ShelX97 (**1**),[62] the XTAL (**2**−**4**)[63] system, and ORTEP[64] program. CCDC-704382 to CCDC-704385 contain the supplementary crystallographic data for **1**, **2**, **3**, and **4** respectively. The CIF files can be obtained free of charge via www.ccdc.cam.ac.uk/conts/retrieving.html (or from the Cambridge Crystallographic Data Centre, 12 Union Road, Cambridge CB2 1EZ, UK; fax: (+ 44) 1223−336−033 or deposit@ccdc.cam.ac.uk).

Comments on the Crystal Structure of 1. The hydrogen atoms were observed and refined with U_{iso} = 0.0403 Å^2, except for the methyl groups (ligand and nitromethane solvent molecules), for which the atomic positions of the hydrogen atoms were calculated. The nitromethane molecule was refined on two sites possessing a common methyl group and with restraints on bond lengths and bond angles. One oxygen atom from water molecule coordinated to the metal atom was split into two positions (O005a and O005b) with population parameters (PP) = 0.5. The O4 atom showed large atomic displacement parameter, but attempts to refine it on two different atomic sites did not improve convergence.

Comments on the Crystal Structure of 2. All non-hydrogen atoms (57) were refined with anisotropic atomic displacement parameters. The hydrogen atoms were observed and refined with U_{iso} = 0.04 Å^2, except for the methyl groups (H18−H26), for which the atomic positions of the hydrogen atoms were calculated and fixed during the refinement. Eleven hydrogen atoms were refined with restraints on bond lengths.

Comments on the Crystal Structure of 3. The atomic positions of the hydrogen atoms were calculated and refined with restraints on bonds lengths and bond angles and with U_{iso} fixed (0.038 Å^2). The ionic triflate anion, which was not involved in hydrogen bonds (Figure S3, Supporting Information) was disordered and refined with restraints on bond distances and bond angles (with U_{iso} = 0.07 Å^2) on two sites with PP = 0.45/0.55. The maximum of the residual electronic density (3 electrons) was located around this disordered anion. All other non-hydrogen atoms were refined with anisotropic atomic displacement parameters.

Comments on the Crystal Structure of 4. The hydrogen atoms were placed in calculated positions and contributed to F_c calculations. The three acetonitrile solvent molecules were refined with isotropic atomic displacement parameters. The poor R_{int} factor was the result of the weak diffraction intensity at high 2Θ, which probably resulted from disorder (or loss) of solvent (the structure contained solvent accessible voids of 62 Å^3, but the residual electron density map contained no peaks above 1.4 e Å^{-3}). The hydrogen atoms of the free water molecule as well as those of the acetonitrile solvent molecules were not included in the refinement process (their inclusion did not improve the convergence).

Spectroscopic and Analytical Measurements. Electronic spectra in the UV−vis were recorded at 20 °C from solutions with a Perkin-Elmer Lambda 900 spectrometer using quartz cells of 0.1 and 1 mm path length. Spectrophotometric titrations were performed with a J&M diode array spectrometer (Tidas series) connected to an external computer. In a typical experiment, 50 mL of $L2^a$ in CH_3CN (2×10^{-4} mol dm^{-3}) were titrated at 20 °C with a solution of $LnX_3\cdot xH_2O$ (10^{-3} mol dm^{-3}) in the same solvent under an inert atmosphere. After each addition of 0.10 mL, the absorbance was recorded using Hellma optrodes (optical path length 0.1 cm) immersed in the thermostatted titration vessel and connected to the spectrometer. Mathematical treatment of the spectrophotometric data

(61) Altomare, A.; Burla, M. C.; Camalli, M.; Cascarano, G.; Giacovazzo, C.; Guagliardi, A.; Moliterni, G.; Polidori, G.; Spagna, R. *J. Appl. Crystallogr.* **1999**, *32*, 115.
(62) Sheldrick, G. M. *SHELXL97 Program for the Solution and Refinement of Crystal Structures*; University of Göttingen: Göttingen, Germany, 1997.
(63) *XTAL 3.2 User's Manual*; Hall, S. R., Flack, H. D., Stewart, J. M., Eds.; Universities of Western Australia and Maryland: 1989.
(64) Johnson, C. K. *ORTEP II*; Report ORNL-5138;Oak Ridge National Laboratory: Oak Ridge, TN, 1976.

Table 10. Summary of Crystal Data, Intensity Measurement, and Structure Refinement for $[Lu(\mathbf{L2^h})(H_2O)_5]Cl_3 \cdot CH_3NO_2$ (**1**), $[Lu(\mathbf{L2^a})(Otf)_3(CH_3CN)(H_2O)]$ (**2**), $[Lu(\mathbf{L2^a})_2(Otf)(H_2O)](Otf)_2$ (**3**), and $[Lu_2(\mathbf{L2^a})_3(SCN)_6] \cdot H_2O \cdot 3CH_3CN$ (**4**)

compound	**1**	**2**	**3**	**4**
formula	$C_{26}H_{35}Cl_3LuN_6O_9$	$C_{28}H_{26}F_9LuN_6O_{10}S_3$	$C_{49}H_{44}F_9LuN_{10}O_{10}S_3$	$C_{81}H_{63}Lu_2N_{24}OS_6$
fw	856.9	1048.7	1375.1	1931.0
cryst syst	orthorhombic	monoclinic	monoclinic	orthorhombic
space group	$P2_12_12_1$	$P2_1/n$	$P2_1/n$	$Pbca$
a (Å)	8.2589(3)	8.1253(4)	12.6659(5)	22.8555(9)
b (Å)	17.8918(10)	22.0172(11)	15.9008(7)	26.5434(12)
c (Å)	22.0679(9)	20.4872(12)	27.1647(13)	28.6078(12)
α (deg)	90	90	90	90
β (deg)	90	100.471(7)	94.329(5)	90
γ (deg)	90	90	90	90
V (Å^3)	3260.9(3)	3604.1(3)	5455.3(4)	17355.3(1.3)
Z	4	4	4	8
cryst size (mm)	0.05 × 0.08 × 0.274	0.11 × 0.15 × 0.31	0.14 × 0.15 × 0.24	0.07 × 0.16 × 0.26
d_{calcd} (Mg m^{-3})	1.748	1.933	1.674	1.478
μ(Mo Kα) (mm^{-1})	3.33	3.02	2.02	2.46
T_{min}, T_{max}	0.7302, 0.8543	0.5846, 0.7329	0.6542, 0.7907	0.6542, 0.7907
2θ max (deg)	51.9	58.6	53.9	51.6
no. reflns collected	23224	49598	61193	117440
no. independent reflns	6179	8997	11712	16880
criterion (q) for obsd reflns[a,b]	4	4	3	3
no. of obsd[a] (used)[b] reflns	5627 (6179)	6651 (6827)	8063 (8331)	7379 (11842)
no. of variables	503	565	847	964
weighting scheme p[c]	g	0.0002	0.0009	0.0002
max and min $\Delta\rho$ (e Å^{-3})	0.53, −0.48	2.19, −1.12	3.06, −3.18	1.41, −2.09
Flack parameter x	0.067(6)			
GOF (F)[d] (all data)	0.98(1)	1.27(1)	1.19(1)	0.790(4)
R[e], ωR[f] (all data)	0.0228, 0.039	0.039, 0.035	0.063, 0.057	0.094, 0.041
R[e], ωR[f] (reflns used)	0.0188, 0.039	0.028, 0.032	0.047, 0.057	0.036, 0.037

[a] $|F_o| > q\sigma(F_o)$. [b] Used in the refinements (including reflns with $|F_o| \le q\sigma(F_o)$ if $|F_c| > |F_o|$). [c] $\omega = 1/[\sigma^2(F_o) + p(F_o)^2]$. [d] $S = [\Sigma\{((F_o - F_c)/\sigma(F_o))^2\}/(N_{ref} - N_{var})]^{1/2}$. [e] $R = \Sigma||F_o| - |F_c||/\Sigma|F_o|$. [f] $\omega R = [\Sigma(\omega|F_o| - |F_c|)^2/\Sigma\omega|F_o|^2]^{1/2}$. [g] $\omega = 1/[\sigma^2(F_o)^2 + (0.0196p)^2$, where $p = [(F_o)^2 + 2(F_c)^2]/3$.

was performed with factor analysis[65] and with the SPECFIT program.[66,67] ^{1}H NMR spectra were recorded at 25 °C on a Bruker Avance 400 MHz. Chemical shifts are given in parts per million (ppm) with respect to TMS. Diffusion experiments were recorded at 400-MHz-proton-Larmor frequency at room temperature. The sequence corresponds to Bruker pulse program *ledbpgp2s*[68] using stimulated echo, bipolar gradients, and longitudinal eddy current delay as z filter. The four 2 ms gradients pulses have sine-bell shapes and amplitudes ranging linearly from 2.5 to 50 G/cm in 16 steps. The diffusion delay was 100 ms and the number of scan 16. The processing was done using a line broadening of 5 Hz and the diffusion rates calculated using the Bruker processing package. Elemental analyses were performed by Dr. H. Eder from the Microchemical Laboratory of the University of Geneva. Least-squares fitting methods and spectral deconvolutions were implemented in Excel, Mathematica, and MATLAB.

Conclusion

The bond valence method is particularly efficient for comparing metal−ligand affinities in the solid state along the complete lanthanide series without resorting to tedious scaling processes considering specific change in coordination numbers and in metallic ionic radii. When analyzing the lanthanide complexes of the archetypal tridentate aromatic ligands **L1** and **L2** in the solid state, we can conclude that (1) only complexes with **L2** display metal−ligand affinity which can be tuned with stoichiometry, (2) the Ln−**L2** affinity decreases with increasing Ln/**L2** stoichiometry because of distortion of the ligands produced by rotations about the interannular bonds, (3) the oxophilicity of Ln(III) follows the expected trend $\nu_{O-H2O} \approx \nu_{O\text{-}Otf} > \nu_{O\text{-}CH3OH} \approx \nu_{O\text{-}NO3} > \nu_{O\text{-}ClO4} > \nu_{N\text{-}CH3CN}$, and (4) NCS^- is a strong N-donor for Ln(III). The reduced affinity of **L2** for Ln(III) with increasing Ln:**L2** stoichiometry is maintained in solution and can be quantified in acetonitrile by using the site binding model. We systematically found repulsive interligand interactions ($2 \le \Delta E^{L,L} \le 9$ kJ/mol; average 5(2) kJ/mol for $\mathbf{L2^a}$), which contribute to destabilize the successive complexes by 0 (Ln/$\mathbf{L2^a}$ = 1:1), 5 (Ln/$\mathbf{L2^a}$ = 1:2), and 15 kJ/mol (Ln/$\mathbf{L2^a}$ = 1:3). Interestingly, this repulsive parameter can be modulated by using simple steric constraints and it reaches $10 \le \Delta E^{L,L} \le 12$ kJ/mol for the crowded ligands $\mathbf{L2^{o-q}}$. However, direct comparisons between metal−ligand affinities in the solid state and in solution remain limited by a reliable interpretation of solvent effects. In this context, we notice that the bond valence $\nu_{N\text{-ligand}}$ in the solid state is not very sensitive to the nature of the rest of the coordination sphere for a given Ln/**L2** stoichiometry, while the thermodynamic formation constants decreases by 2−3 orders of magnitude when coordinated triflates are replaced with nitrates or with thiocyanates in 1:1 complexes (Table 7). This effect obviously relies on different solvation processes affecting the reactants and products, a phenomenon which can be exploited, at least empirically, for preparing complexes with controlled stoichiometries. The surprising, but considerable decrease of the dimerization constant leading to [Eu_2-

(65) Malinowski, E. R.; Howery, D. G. *Factor Analysis in Chemistry*; Wiley: New York, 1980.
(66) Gampp, H.; Maeder, M.; Meyer, C. J.; Zuberbühler, A. *Talanta* **1985**, *32*, 1133.
(67) Gampp, H.; Maeder, M.; Meyer, C. J.; Zuberbühler, A. *Talanta* **1986**, *33*, 943.
(68) Wu, D.; Chen, A., Jr *J. Magn. Reson. A* **1995**, *155*, 260.

($\mathbf{L2^q}$)$_2$(NO_3)$_6$] in going from CD_2Cl_2 to $CDCl_3$ further confirms the crucial role played by minor solvent changes in lanthanide coordination chemistry, even with rather rigid and preorganized ligands in organic solvents.

In conclusion, both terpyridine (**L1**) and 2,6-bis(benzimidazole-2-yl)pyridine (**L2**) ligands are adapted for producing planar 1:1 and helical 1:2 and 1:3 complexes with trivalent lanthanides, but the distal coordinated five-membered rings in **L2** produce a coordination cavity better suited for fine-tuning mediated by interligand effects. The successive fixation of **L2** ligands to Ln(III) is unambiguously anticooperative and the stoichiometry of the final complexes can be controlled by a judicious combination of specific interligand ($u^{L,L}$) and solvation (f^{Ln}_{N3}) contributions.

Acknowledgment. Financial support from the COST D31 action and from the Swiss National Science Foundation is gratefully acknowledged.

Supporting Information Available: Tables (S1−S26) and Figures (S1−S6) corresponding to thermodynamic and structural modeling, spectroscopic analyses, and fitting processes. This material is available free of charge via the Internet at http://pubs.acs.org.

IC801908C